J. Fluid Mech. (1995), *vol.* 285, *pp.* 121–158

Spatial bifurcations of interfacial waves when the phase and group velocities are nearly equal

By T. J. BRIDGES[1], P. CHRISTODOULIDES[2] AND F. DIAS[2]

[1] Department of Mathematics, University of Surrey, Guildford, Surrey GU2 5XH, UK

[2] Institut Non-Linéaire de Nice, Université de Nice – Sophia Antipolis, 1361 route des Lucioles, F-06560 Valbonne, France

(Received 4 February 1994 and in revised form 7 September 1994)

Steady waves at the interface between two immiscible and inviscid fluids of differing density are studied. The governing equations are reformulated as a spatial Hamiltonian system leading to new variational principles for uniform states and travelling waves. Analytical methods based on the properties of the Hamiltonian structure and numerical methods are used to find new branches of steady nonlinear interfacial waves in the neighbourhood of the singularity $c = c_g$. While the water-wave problem (upper fluid density negligible) near this singularity has received considerable attention the results for interfacial waves present some new features. The branches of travelling waves when plotted in $(\tilde{F}, \tilde{S})$-space, where $\tilde{F}$ and $\tilde{S}$ are related to the energy flux and flow force respectively, show new bifurcations in the context of hydrodynamic waves even at very low amplitudes. The secondary bifurcations are explained by a spatial analogue of the superharmonic instability. An interesting analogy is also found between the spatial bifurcations of travelling waves and the Kelvin–Helmholtz instability. The new branches of waves occur at physically realizable values of the parameters and therefore could have implications for interfacial waves in applications.

1. Introduction

Waves at the interface between two fluids are of fundamental interest in oceanographic and atmospheric flows and their modelling, as well as in theoretical fluid mechanics. One of the best-known examples of two-layer oceanographic flow is the flow through the Strait of Gibraltar where evaporation over the Mediterranean forces an inflow of fresher water in an upper layer from the Atlantic and an outflow of saltier water in a deeper layer from the Mediterranean (see Bryden & Kinder 1991 for a review). Observations of the flow through the Strait of Gibraltar indicate the presence of two locations where critical flows occur (see Appendix C). Critical flows are an essential feature in the study of two-layer flows, since they can bifurcate into solitary waves and, in some degenerate cases, into fronts. One of the best-known experiments on two-layer fluids in the presence of interfacial tension is that by Thorpe (1969), which consisted in tilting a tube filled with two immiscible fluids and returning it to its horizontal position. Various wavy phenomena can occur along the interface, such as propagating Holmboe waves (see for example the recent paper by Pouliquen, Chomaz & Huerre 1994). In applications and experiments the density gradient is often sharp enough so that the two-fluid system, where the two fluids are treated as distinct and immiscible with a discontinuity in the density across the interface, provides a good model (see for example Koop & Redekopp 1981). In this paper a new formulation and new analytic and numerical results re presented for steady capillary–gravity interfacial

waves. This new formulation, which is quite general, also provides new tools to study subcritical as well as critical two-layer flows.

The most fundamental waves at the interface between two fluids are waves that are steady relative to a moving frame of reference. The governing equations for steady interfacial waves are first formulated as a Hamiltonian system in space of the form

$$\boldsymbol{K}(\boldsymbol{Z})\,\boldsymbol{Z}_x = \nabla \bar{S}(\boldsymbol{Z}), \tag{1.1}$$

where $\boldsymbol{Z}$ is a vector containing the dependent variables (velocity potential in the upper and lower layers, interface position, etc.), $\boldsymbol{K}(\boldsymbol{Z})$ is a skew-symmetric operator and $\bar{S}(\boldsymbol{Z})$ is the flow force for the interfacial wave problem in terms of the $\boldsymbol{Z}$-coordinates. This spatial Hamiltonian structure is not to be confused with the Hamiltonian structure for the time-dependent water-wave problem (Zakharov 1968; Benjamin & Olver 1982) or the time-dependent interfacial-wave problem (Benjamin & Bridges 1992; Dias & Bridges 1994). The idea of reformulating steady wave problems as a spatial Hamiltonian system has been an area of recent and active interest (Benjamin 1984; Mielke 1991; Baesens & MacKay 1992; Bridges 1992*a*, *b*, 1994). The advantage of a Hamiltonian structure is that one can appeal to established general results on Hamiltonian systems to reveal new results for waves.

There are two important physical quantities associated with linear waves: their phase velocity c and their group velocity c_g. When the two velocities are equal, or nearly equal, the nonlinear problem becomes quite rich. In particular, solitary waves can bifurcate either from a critical flow (if the wave such that $c = c_g$ is a long wave with zero wavenumber) or from a train of infinitesimal periodic waves (if the wave such that $c = c_g$ is a wave with non-zero wavenumber). In this paper, motivated by the Hamiltonian structure of the steady wave problem, we obtain new results on the bifurcation of steady waves near the singularity $c = c_g$ with non-zero wavenumber k. The dispersion relation for capillary–gravity waves travelling at the interface between two unbounded fluids of density ρ (lower fluid) and ρ' (upper fluid) can be written as

$$c^2 = \frac{(\rho-\rho')\,g}{(\rho+\rho')\,k} + \frac{\sigma k}{\rho+\rho'}, \tag{1.2}$$

where g is the acceleration due to gravity and σ the coefficient of interfacial tension. The dispersion curve (see figure 1*a*) exhibits a minimum, which is denoted by (k_0, c_0). Since

$$\frac{\mathrm{d}c}{\mathrm{d}k} = \frac{1}{k}\frac{\mathrm{d}(kc)}{\mathrm{d}k} - \frac{c}{k} = -\frac{1}{k}(c - c_g)$$

is zero at (k_0, c_0), it follows that the group velocity c_g is equal to the phase velocity at that minimum. From now on, the $c = c_g$ singularity will refer to the case corresponding to the minimum of the dispersion curve, and not to the long-wave case.

For classical water waves, which correspond to $\rho' = 0$, the ramifications of the singularity $c = c_g$ for the linear problem have been studied by Whitham (1974, pp. 451–452). When a current U is present the singularity becomes $c_g + U = c$ and in the study of wave–current interaction this singularity corresponds to stopping velocities (cf. Gargett & Hughes 1972; Peregrine 1976, p. 52; Peregrine & Thomas 1979, §5). Gargett & Hughes (1972, figures 1, 2) note that stopping velocities lead to interesting interfacial wave patterns. The nonlinear problem near $c = c_g$ for the classic water-wave problem has received considerable attention recently (cf. Hogan 1983; Iooss & Kirchgässner 1990, Bridges 1992*b*, §5; Vanden-Broeck & Dias 1992; Dias & Iooss 1993; Akylas 1993; Longuet-Higgins 1993 and references therein). It has been found

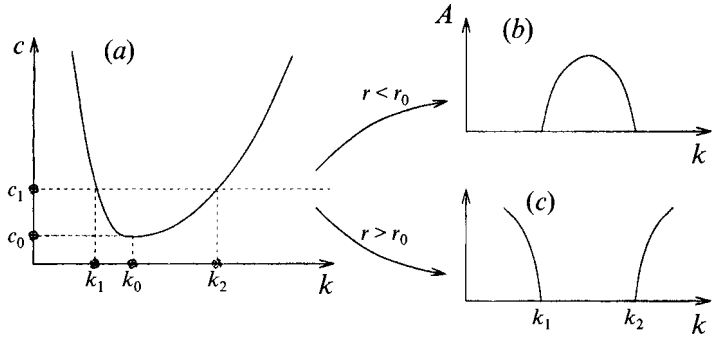

FIGURE 1. Local bifurcation of periodic travelling waves near the critical point (k_0, c_0): (*a*) dispersion curve for the linear problem, (*b*) global loop in the nonlinear problem when $r < r_0 = \sqrt{5}/4$ and $c > c_0$, (*c*) branches of nonlinear travelling waves when $r > r_0$ and $c > c_0$.

for example that solitary waves which look like steady wave packets bifurcate from the trivial solution at the critical point (k_0, c_0). Working with a model equation, Benjamin (1992) showed that such solitary waves should also exist at the interface between two fluids. From a physical point of view, these waves can be approximated as steady solutions of the nonlinear Schrödinger equation, i.e. solutions for which the wave envelope and the oscillations inside travel at the same speed.

However, new features occur in the nonlinear problem near the singularity $c = c_g$ when the upper fluid density is no longer negligible. This can already be seen when considering the weakly nonlinear branches of travelling waves. In figures 1(*b*) and 1(*c*) the branches of weakly nonlinear periodic travelling waves are plotted as a function of k, the wavenumber, for fixed c. In figure 1 A is some measure of the amplitude of the wave, typically the amplitude of the first Fourier coefficient of the interfacial displacement. The branching diagrams for the weakly nonlinear travelling waves depend on the density difference. Let

$$r = \frac{\rho - \rho'}{\rho + \rho'} \quad \text{and} \quad r_0 = \frac{\sqrt{5}}{4}.$$

The parameter r is the normalized density difference between the two fluids and r_0 is a critical value of r, which will be determined analytically below. When $r > r_0$, which includes the case where the upper fluid density is negligible, the two branches of waves bifurcate in opposite directions. In other words the wavelength of a wave bifurcating from $k_1 < k_0$ increases with amplitude whereas the wavelength of a wave bifurcating from $k_2 > k_0$ decreases with amplitude. When $r < r_0$ there is a dramatic change: the two branches are globally connected. These results will be confirmed analytically in §3 and numerically in §5.

Figure 1 does not tell the whole story, however, and here the spatial Hamiltonian structure is helpful in analysing the significance of the globally connected branches. The importance of the spatial Hamiltonian structure can already be seen in the linear problem. At the end of §2 the linearization of the spatial dynamical system (1.1) is studied. There it is shown that the point $c = c_0$ corresponds to a collision of spatial eigenvalues of opposite signature (cf. figure 4) that is reminiscent of instability in a time-evolution Hamiltonian system. It is interesting to note that this interpretation of the linear problem near the singularity $c = c_g$ gives a precise formulation of an observation of Gargett & Hughes. Gargett & Hughes (1972, p. 179) note that at the singularity $c_g + U = c$ two wavenumbers which were real and distinct on one side

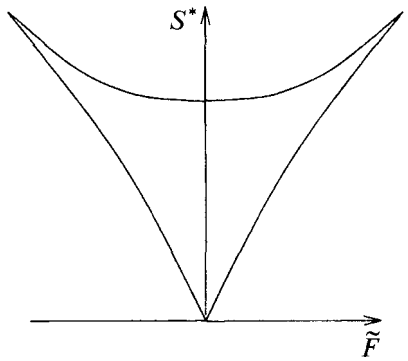

FIGURE 2. Global branch of nonlinear travelling waves in the $(\tilde{F}, S^*)$-invariant space when $r < r_0$ and $c > c_0$.

coalesce and become complex on the other. Indeed figure 4 represents, from a spatial dynamics viewpoint, precisely this observation. By further appeal to the Hamiltonian structure we will be able to obtain further results on the nonlinear aspects of the problem near the singularity.

One way to obtain further information about the nonlinear branches of waves and secondary bifurcations is to plot the branches of waves in parameter space using the natural parameters from the Hamiltonian structure. The behaviour along the globally connected branch of travelling waves is smooth in the (k, A)-plane as shown in figure 1(*b*), where $c > c_0$ and $r < r_0$. However, the interaction between the capillary wave $(k \to k_2)$ and the gravity wave $(k \to k_1)$ along the branch in figure 1(*b*) is revealed as a cusp when plotted in the proper space. But it is not obvious *a priori* which are the proper parameters. The natural parameters turn out to be values of the level sets for the following functionals evaluated along a branch of travelling waves:

$$\left.\begin{aligned} \bar{S} &= \int_{-\infty}^{\eta} \tfrac{1}{2}\rho(\phi_x^2-\phi_y^2)\,\mathrm{d}y + \int_{\eta}^{\infty} \tfrac{1}{2}\rho'(\phi_x'^2-\phi_y'^2)\,\mathrm{d}y - \tfrac{1}{2}(\rho-\rho')\,g\eta^2 + \sigma - \frac{\sigma}{(1+\eta_x^2)^{1/2}}, \\ \bar{F} &= \int_{-\infty}^{\eta} \rho\phi_x(\phi_x-c)\,\mathrm{d}y + \int_{\eta}^{\infty} \rho'\phi_x'(\phi_x'-c)\,\mathrm{d}y + \frac{\sigma\eta_x^2}{(1+\eta_x^2)^{1/2}}, \end{aligned}\right\} \tag{1.3}$$

where ϕ and ϕ' are the velocity potentials in the lower and upper fluid layers. The first functional $\bar{S}$, which is the flow force relative to the moving frame, is in fact an absolute spatial invariant ($\mathrm{d}\bar{S}/\mathrm{d}x = 0$) for uniformly travelling waves (cf. Benjamin 1984). $-\bar{S}$ can be described as the *wave resistance* of a steady wave train relative to a state of rest. The second functional is related, but not equal, to the energy flux: explicitly $\bar{F} = F/c - cI$ where F is the energy flux relative to the moving frame and I is the impulse. The functional $\bar{F}$ is the *action* functional for the spatial Hamiltonian formulation (it can also be related to Whitham's action *flux*). There has been much work on the role of integrals for the classic water-wave problem and the interfacial-wave problem, and the invariant $\bar{S}$ and the integral $\bar{F}$ (or its average over a wavelength $\tilde{F}$) are well-known (cf. Pullin & Grimshaw 1983, equation (17)), but the importance of displaying the branches of travelling waves, parametrized by wavenumber, in terms of the values of the functionals $\tilde{F}$ and $\bar{S}$ has not previously been recognized.

If the wavelength is normalized to 2π, the wavenumber appears as a Lagrange multiplier in the analysis. In figure 2 the branch of waves along the global loop of figure 1(*b*) is plotted in the $(\tilde{F}, S^*)$-plane where $S^* = \bar{S} - k_0\tilde{F}$. The points k_1 and k_2 (where

$A = 0$) lie at the origin and the point $k = k_0$ with $A \neq 0$ corresponds to the point on the vertical axis. There are two interesting points – one between k_1 and k_0 and one symmetrically placed between k_0 and k_2 – which show up as cusp points in the $(\tilde{F}, S^*)$-plane (the choice of the $(\tilde{F}, S^*)$-plane rather than the $(\tilde{F}, \bar{S})$-plane allows a better visualization of the cusps). It is important to note that this picture is valid for all density ratios such that $0 < r < r_0$.

In the linear problem the coalescence of a gravity wave and a capillary wave results in the critical point (k_0, c_0) where the phase velocity equals the group velocity. In the nonlinear problem the interaction of a gravity wave and a capillary wave along the branch of nonlinear states of figure 1(*b*) results in the cusp points. The cusp points are important because they carry information about secondary spatial bifurcations. In fact the cusp points are spatial analogues of the superharmonic instability! In §4 we adapt the Hamiltonian theory of the superharmonic instability due to Saffman (1985) to the spatial setting. It is shown that the cusp points correspond to spatial Floquet multipliers entering or leaving the unit circle. The position of the Floquet multipliers then leads to information about secondary bifurcation to new families of periodic and solitary waves. Motivated by the present study, Dias & Iooss (1994) have shown that dark solitary waves exist along the part of the branch connecting the cusp points. These are solitary waves that are biasymptotic to the travelling waves along the globally connected branch in figure 1(*b*), between the two cusp points (see also figure 8).

A second effect of the interaction of capillary and gravity effects along the global branches of waves, particularly when $r \approx r_0$, is the appearance of a bifurcation point and a new branch of waves that does not connect with the trivial state. Analytical and numerical results are presented for the disconnected branches by working in a neighbourhood of parameter space with $|r - r_0|$ small in §3 and in §5. Numerical results indicate that the new disconnected branches persist for larger regions of parameter space and therefore should have implications for interfacial waves in applications.

In §2 the governing equations for uniformly travelling capillary–gravity waves are presented and reformulated as a spatial Hamiltonian system. In terms of the spatial Hamiltonian structure, the critical point (k_0, c_0) shows up in the linear problem as a collision of purely imaginary (spatial) eigenvalues of opposite signature. The collision of eigenvalues has been well-studied in the finite-dimensional Hamiltonian systems literature (van der Meer 1985; Bridges 1990, 1991). Recourse to the Hamiltonian theory is made here to analyse the spatial bifurcations in the interfacial-wave problem.

In §3 a new variational principle based on the spatial Hamiltonian structure and weakly nonlinear theory are used to find all local bifurcations of travelling waves near the point (k_0, c_0) when the density difference r is near the singular value r_0. The unfolding of this singularity contains globally connected branches, bifurcation points at finite amplitude and isolated branches. It is remarkable that such structure can be found analytically. The (r, c) parameter space near (r_0, c_0) is divided into five regions, each of which having distinct bifurcation diagrams. In §4 the role of the integrals $\bar{S}, \tilde{F}$ and $\bar{Q}_{tot}$ (total mass flux) in the spatial bifurcations is considered.

In §5 the bifurcations of finite-amplitude waves are studied numerically. For the numerical computations we use a scheme based on Fourier collocation, originally proposed by Saffman & Yuen (1982). The numerical calculations confirm the analytic predictions and extend the results to finite amplitude. The numerical calculations show that the disconnected branches, which arise through a bifurcation point (the curve B_1 in figure 6), persist for large regions of (c, r) parameter space. As far as we are aware these branches have not been previously found. Here they are studied by combining the analytic predictions with numerical continuation.

There is an interesting similarity between the singularity (k_0, c_0) for steady waves and the Kelvin–Helmholtz instability for time-dependent interfacial waves with a current. This correspondence is the subject of §6.

A discussion of problems that remain open (in particular the problem of what happens to the solitary waves with oscillating tails bifurcating at the critical point, as the density ratio approaches the critical density ratio) and of physical consequences of the results described in the preceding sections are provided in §7.

In Appendix A the spatial invariants (flow force, mass fluxes) are derived from the conservation laws. In Appendix B the details of the construction of the spatial Hamiltonian structure are presented. In Appendix C, we present a novel variational principle for uniform flows that includes a new definition for criticality of uniform flows. Finally, in Appendix D, a new variational principle for periodic travelling waves that includes a characterization of the coupled mean flow is presented.

2. Interfacial waves and spatial Hamiltonian structure

The primary purpose of the present study is to analyse steady waves at the interface between two stably stratified inviscid incompressible fluids. For uniformly travelling waves, a frame of reference can be chosen in which the mean of the horizontal velocity is zero (or equal to $-c$ if the frame of reference moves with the wave) and the mean height of the interface is zero, in which case Bernoulli's constant is non-zero. Alternatively, one can choose Bernoulli's constant to be zero with a non-zero mean height. We will make the latter choice below. It will be shown that the problem of steady waves can be formulated as a spatial Hamiltonian problem. Such a formulation can be generalized to uniform flows, waves in the presence of currents, waves coupled with a mean flow. Some extensions are provided in Appendices C and D.

The problem is first formulated for a channel of finite height as shown in figure 3. The channel height is $h+h'$ and the interface $y = \eta(x)$ separates two fluids of density ρ and ρ' with $\rho > \rho' > 0$. the flow field is two-dimensional and irrotational in each layer with velocity potentials ϕ and ϕ' satisfying

$$\left.\begin{aligned} \Delta\phi \overset{\text{def}}{=} \frac{\partial^2\phi}{\partial x^2}+\frac{\partial^2\phi}{\partial y^2} = 0 \quad \text{for} \quad -h < y < \eta(x), \\ \Delta\phi' \overset{\text{def}}{=} \frac{\partial^2\phi'}{\partial x^2}+\frac{\partial^2\phi'}{\partial y^2} = 0 \quad \text{for} \quad \eta(x) < y < h', \end{aligned}\right\} \tag{2.1}$$

with boundary conditions at the upper and lower walls

$$\phi_y = 0 \quad \text{at} \quad y = -h \quad \text{and} \quad \phi'_y = 0 \quad \text{at} \quad y = h'. \tag{2.2}$$

At the interface there are two kinematic conditions

$$\left.\begin{aligned} (\phi_x - c)\,\eta_x - \phi_y = 0 \\ (\phi'_x - c)\,\eta_x - \phi'_y = 0 \end{aligned}\right\} \quad \text{at} \quad y = \eta(x). \tag{2.3}$$

The dynamic condition at the interface is then

$$-c(\rho\phi_x - \rho'\phi'_x)+\tfrac{1}{2}\rho(\phi_x^2+\phi_y^2)-\tfrac{1}{2}\rho'(\phi_x'^2+f_y'^2)+(\rho-\rho')\,g\eta-\sigma w_x = 0,$$

or

$$\tfrac{1}{2}\rho[(\phi_x - c)^2+\phi_y^2]-\tfrac{1}{2}\rho'[(\phi'_x - c)^2+\phi_y'^2]+(\rho-\rho')\,g\eta-\sigma w_x = R, \tag{2.4}$$

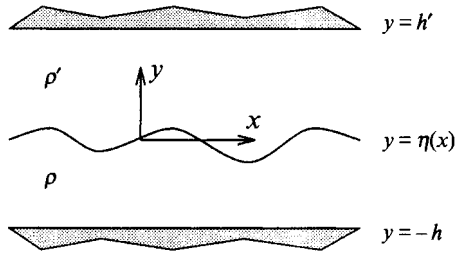

FIGURE 3. Schematic of the two-layer fluid problem.

with $R = \frac{1}{2}(\rho - \rho')c^2$. The symbols g and σ denote the acceleration due to gravity and the coefficient of interfacial tension respectively, and

$$w = \eta_x/(1+\eta_x^2)^{1/2}. \tag{2.5}$$

The set (2.1)–(2.4) with the definition (2.5) are the governing equations for steady interfacial waves. Associated with the set of equations are spatial invariants. For example the flow force and the mass fluxes in the upper and lower layers are independent spatial invariants. The spatial invariants for the above system are derived in Appendix A from the mass, impulse and energy conservation laws for the time-dependent problem.

The governing equations can be reformulated as a Hamiltonian system with evolution in the x-direction.

Introduce weighted velocities

$$u = \rho(\phi_x - c), \quad u' = \rho'(\phi'_x - c), \tag{2.6a}$$

with interface values

$$u = u|_{y=\eta(x)} \quad u' = u'|_{y=\eta(x)}, \tag{2.6b}$$

as well as interface values for the potentials

$$\Phi(x) = \phi(x,y)|_{y=\eta(x)}, \quad \Phi'(x) = \phi'(x,y)|_{y=\eta(x)}. \tag{2.7}$$

It is then immediately obvious that

$$\Phi_x = [\phi_x + \phi_y \eta_x]|_{y=\eta(x)} \quad \text{and} \quad \Phi'_x = [\phi'_x + \phi'_y \eta_x]|_{y=\eta(x)}. \tag{2.8}$$

In terms of the above coordinates the governing equations are reformulated as follows. The kinematic conditions (2.3) can be rewritten as

$$\left.\begin{aligned} u\eta_x - \rho\phi_y &= 0 \\ u'\eta_x - \rho'\phi'_y &= 0 \end{aligned}\right\} \quad \text{at} \quad y = \eta(x). \tag{2.9}$$

In order to reformulate the dynamic condition we use the following identities which are verified using (2.6)–(2.9):

$$\left.\begin{aligned} \tfrac{1}{2}\rho[(\phi_x - c)^2 + \phi_y^2] &= u\Phi_x - \frac{1}{2}\left[\frac{1}{\rho}u^2 + \rho\phi_y^2\right]\Big|_{y=\eta} - cu, \\ \tfrac{1}{2}\rho'[(\phi'_x - c)^2 + \phi'^2_y] &= u'\Phi'_x - \frac{1}{2}\left[\frac{1}{\rho'}u'^2 + \rho'\phi'^2_y\right]\Big|_{y=\eta} - cu'. \end{aligned}\right\} \tag{2.10}$$

It is now straightforward to verify that the governing equations (2.1), (2.3) and (2.4) can be reformulated as

$$\left.\begin{aligned} &-u\eta_x = -\rho\phi_y|_{y=\eta}, \quad u'\eta_x = \rho'\phi'_y|_{y=\eta}, \\ &u\Phi_x - u'\Phi'_x - \sigma w_x = R-(\rho-\rho')g\eta + \frac{1}{2}\left[\frac{1}{\rho}u^2+\rho\phi_y^2-\frac{1}{\rho'}u'^2-\rho'\phi_y'^2\right]\Big|_{y=\eta} + cu - cu', \\ &\sigma\eta_x = \frac{\sigma w}{(1-w^2)^{1/2}}, \quad -u_x = \rho\phi_{yy}, \quad \phi_x = \frac{u}{\rho}+c, \quad -u'_x = \rho'\phi'_{yy}, \quad \phi'_x = \frac{u'}{\rho'}+c. \end{aligned}\right\} \tag{2.11}$$

The reformulation (2.11) leads to an interesting variational structure for the equations governing steady waves. Let $\boldsymbol{Z}$ represent the vector-valued set of dependent variables and introduce the $\boldsymbol{Z}$-dependent operator $\boldsymbol{K}(\boldsymbol{Z})$,

$$\boldsymbol{Z} = \begin{pmatrix} \Phi \\ \Phi' \\ \eta \\ w \\ \phi \\ u \\ \phi' \\ u' \end{pmatrix} \quad \text{and} \quad \boldsymbol{K}(\boldsymbol{Z}) = \begin{pmatrix} 0 & 0 & -u & 0 & 0 & 0 & 0 & 0 \\ 0 & 0 & u' & 0 & 0 & 0 & 0 & 0 \\ u & -u' & 0 & -\sigma & 0 & 0 & 0 & 0 \\ 0 & 0 & \sigma & 0 & 0 & 0 & 0 & 0 \\ 0 & 0 & 0 & 0 & 0 & -1 & 0 & 0 \\ 0 & 0 & 0 & 0 & 1 & 0 & 0 & 0 \\ 0 & 0 & 0 & 0 & 0 & 0 & 0 & -1 \\ 0 & 0 & 0 & 0 & 0 & 0 & 1 & 0 \end{pmatrix}. \tag{2.12}$$

Then (2.11) has the representation

$$\boldsymbol{K}(\boldsymbol{Z})\,\boldsymbol{Z}_x = \nabla\bar{S}(\boldsymbol{Z}). \tag{2.13}$$

The left-hand side is verified by writing out $\boldsymbol{K}(\boldsymbol{Z})\,\boldsymbol{Z}_x$ using the definition in (2.12) and comparing with (2.11). On the right-hand side $\nabla\bar{S}$ is the gradient of the flow force $S-cI$. To verify the representation on the right-hand side of (2.13) it is necessary to show that $\bar{S}$ represents the flow force and to introduce an inner product for the definition of the gradient.

The flow force is the steady part of the flux associated with the impulse conservation law (cf. Appendix A) and in terms of the set of $\boldsymbol{Z}$-coordinates is

$$\bar{S}(\boldsymbol{Z}) = \int_{-h}^{\eta}\frac{1}{2}\left[\frac{1}{\rho}(u+\rho c)^2-\rho\phi_y^2\right]dy + \int_{\eta}^{h'}\frac{1}{2}\left[\frac{1}{\rho'}(u'+\rho' c)^2-\rho'\phi_y'^2\right]dy$$
$$-\tfrac{1}{2}(\rho-\rho')g\eta^2+\sigma[1-(1-w^2)^{1/2}]. \tag{2.14}$$

It remains to consider the gradient of the above functional. For eight-component vectors of the form in (2.12), where the first four components are independent of y and the last four depend on the y-cross-section, a suitable inner product is

$$\langle U, V\rangle_\eta = \sum_{j=1}^{4} U_j V_j + \int_{-h}^{\eta}(U_5 V_5 + U_6 V_6)\,dy + \int_{\eta}^{h'}(U_7 V_7 + U_8 V_8)\,dy, \tag{2.15}$$

where the η subscript denotes that the inner product is η-dependent. In terms of the inner product (2.15) it is easily verified that

$$\nabla\bar{S}(\boldsymbol{Z}) \stackrel{\text{def}}{=} \begin{pmatrix} \delta\bar{S}/\delta\Phi \\ \delta\bar{S}/\delta\Phi' \\ \delta\bar{S}/\delta\eta \\ \delta\bar{S}/\delta w \\ \delta\bar{S}/\delta\phi \\ \delta\bar{S}/\delta u \\ \delta\bar{S}/\delta\phi' \\ \delta\bar{S}/\delta u' \end{pmatrix}$$

$$= \begin{pmatrix} -\rho\phi_{y|\,y=\eta} \\ \rho'\phi'_y|_{y=\eta} \\ R-(\rho-\rho')g\eta+\frac{1}{2}\left[\frac{1}{\rho}u^2+\rho\phi_y^2-\frac{1}{\rho'}u'^2-\rho'\phi_y'^2\right]\Big|_{y=\eta}+c(u-u') \\ \sigma w/(1-w^2)^{1/2} \\ \rho\phi_{yy} \\ u/\rho+c \\ \rho'\phi'_{yy} \\ u'/\rho'+c \end{pmatrix}. \quad (2.16)$$

Comparing (2.16) with the right-hand side of (2.11) completes the verification of the representation (2.13).

The system (2.13) is a spatial Hamiltonian system with the skew-symmetric operator on the left-hand side. It is interesting that the representation (2.13) of the governing equations shows explicitly the importance of the flow force whereas this information is only implicit in the governing equations (2.1)–(2.5). The abstract properties of the system (2.13) and some of the consequences of the Hamiltonian structure are considered in Appendix B. The operator $\boldsymbol{K}(\boldsymbol{Z})$ is not invertible and such systems, although they retain most of the properties of standard Hamiltonian systems, are sometimes called quasi-Hamiltonian systems (Benjamin & Olver 1982, Appendix 1; Benjamin & Bridges 1992, Bridges 1992*b*, equation (3.15)).

The study of steady states by first reformulating the system as a spatial Hamiltonian system has been the subject of recent and active interest (cf. Benjamin 1984; Zufiria 1987; Mielke 1991; Baesens & MacKay 1992; Bridges 1992*a*, *b*, 1994). The advantage of a spatial Hamiltonian formulation is that one can appeal to many known results on Hamiltonian systems to obtain new results and a more complete understanding of steady waves. In particular, a variational principle for periodic uniformly travelling waves will be derived in §3 and used to organize the spatial bifurcation of travelling waves near the critical point where $c = c_g$ for interfacial waves. In §4 the abstract properties of the spatial Hamiltonian structure are used to prove results on the movement of spatial Floquet multipliers leading to information about secondary bifurcations of travelling waves and new families of waves. A similar structure to (2.13) also exists for uniform flows and leads to a variational principle for uniform flows (see Appendix C). A variational principle can also be derived for periodic travelling waves coupled to the mean flow effects (see Appendix D).

For simplicity both layers are now supposed to be of infinite height ($h \to \infty$ and $h' \to \infty$). By treating the governing equations as a spatial Hamiltonian system we

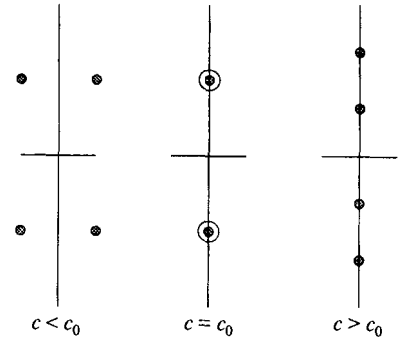

FIGURE 4. Collision of spatial eigenvalues of opposite signature when passing through the critical point (k_0, c_0).

obtain an interesting interpretation of the dispersion relation for waves linearized about the uniform flow. An important point on the dispersion curve is the point where $c = c_g$. In the spatial context the point $c = c_g$ is associated with a spatial collision of eigenvalues (cf. figure 4). This is verified as follows. The linearization of (2.13) results in

$$\boldsymbol{K}_0 \boldsymbol{Z}_x = \boldsymbol{A}\boldsymbol{Z}, \tag{2.17}$$

where

$$\boldsymbol{K}_0 = \boldsymbol{K}(\boldsymbol{Z})|_{u=-\rho c,\, u'=-\rho' c} = \begin{pmatrix} 0 & 0 & \rho c & 0 & 0 & 0 & 0 & 0 \\ 0 & 0 & -\rho' c & 0 & 0 & 0 & 0 & 0 \\ -\rho c & \rho' c & 0 & -\sigma & 0 & 0 & 0 & 0 \\ 0 & 0 & \sigma & 0 & 0 & 0 & 0 & 0 \\ 0 & 0 & 0 & 0 & 0 & -1 & 0 & 0 \\ 0 & 0 & 0 & 0 & 1 & 0 & 0 & 0 \\ 0 & 0 & 0 & 0 & 0 & 0 & 0 & -1 \\ 0 & 0 & 0 & 0 & 0 & 0 & 1 & 0 \end{pmatrix}$$

and

$$\boldsymbol{A}\boldsymbol{Z} \overset{\text{def}}{=} D^2\bar{S}(0)\,\boldsymbol{Z} = \begin{pmatrix} -\rho\phi_y|_{y=0} \\ \rho'\phi'_y|_{y=0} \\ -(\rho-\rho')g\eta \\ \sigma w \\ \rho\phi_{yy} \\ u/\rho \\ \rho'\phi'_{yy} \\ u'/\rho' \end{pmatrix},$$

where u (resp. u') is now equal to $\rho\phi_x$ (resp. $\rho'\phi'_x$) and $w = \eta_x$. To complete the specification of the linear problem we need the far-field boundary conditions ($\phi_y \to 0$ as $y \to -\infty$ and $\phi'_y \to 0$ as $y \to +\infty$) and the compatibility conditions (boundary conditions on ϕ, ϕ' and the constraints (B 7)):

$$\phi|_{y=0} = \Phi, \quad \phi'|_{y=0} = \Phi', \quad \phi_y|_{y=0} + cw = 0, \quad \phi'_y|_{y=0} + cw = 0.$$

Setting $\hat{\boldsymbol{Z}} = \hat{\boldsymbol{Z}}\mathrm{e}^{\mathrm{i}kx} + \text{c.c.}$ results in the eigenvalue problem

$$(\boldsymbol{A} - \mathrm{i}k\boldsymbol{K}_0)\,\hat{\boldsymbol{Z}} = 0$$

with dispersion relation

$$c^2 = \frac{(\rho-\rho')g}{(\rho+\rho')k} + \frac{\sigma k}{\rho+\rho'}. \tag{2.18}$$

The dispersion relation in the (k, c)-plane has been plotted in figure 1(*a*). The point of interest here is the critical point (k_0, c_0) defined by solutions of (2.18) that also satisfy $\mathrm{d}c/\mathrm{d}k = 0$. This results in

$$c_0 = \left(\frac{2\sigma k_0}{\rho+\rho'}\right)^{1/2} \quad \text{and} \quad k_0 = \left(\frac{(\rho-\rho')g}{\sigma}\right)^{1/2}.$$

Before proceeding to analyse the nonlinear problem we re-examine the critical point (k_0, c_0) from a spatial dynamical systems viewpoint. Inverting the dispersion relation (2.18) by letting $\lambda = \mathrm{i}k$ with $\lambda \in \mathbb{C}$ and solving for λ as a function of c yields

$$\lambda = \frac{\rho+\rho'}{2\sigma}[\mathrm{i}c^2 \pm (c_0^4 - c^4)^{1/2}]. \tag{2.19}$$

The complex values of λ given by (2.19) are plotted as functions of c in figure 4. When $c \in \mathbb{R}$ is treated as a control parameter, the spatial eigenvalues pass through, at $c = c_0$, a spatial collision of eigenvalues of opposite signature (see Bridges 1992*b*, §5) for the role of signature and momentum flux sign in such collisions).

The above result is a dynamical systems interpretation of a result first noted by Gargett & Hughes (1972). Gargett & Hughes (1972, p. 179) note that when $c_g + U = c$ two wavenumbers which were real and distinct on one side coalesce and become complex on the other. The Gargett & Hughes description is precisely as shown in figure 4 (within the present context $U = 0$) in going from $c > c_0$ to $c < c_0$. By placing this result in a Hamiltonian spatial context we can appeal in §§3–5 to known results on the nonlinear behaviour of Hamiltonian systems near such a singularity.

3. Bifurcation of travelling waves when c is near c_g

The branches of periodic travelling waves are altered significantly by the singularity $c = c_g$. In this section the branches of travelling waves near $c = c_g$ are constructed using a variational principle based on the spatial Hamiltonian structure. The effect of the singularity $c = c_g$ is already present when $h, h' \to \infty$ and therefore we restrict to this case. Scaling x into kx, so that k appears in the governing equation (2.13), results in

$$k\boldsymbol{K}(\boldsymbol{Z})\boldsymbol{Z}_x = \nabla\bar{S}(\boldsymbol{Z}). \tag{3.1}$$

But letting

$$\bar{F} = \sigma w\eta_x + \int_{-\infty}^{\eta} u\phi_x \,\mathrm{d}y + \int_{\eta}^{\infty} u'\phi_x' \,\mathrm{d}y$$

and noting that $\nabla\bar{F} = \boldsymbol{K}(\boldsymbol{Z})\boldsymbol{Z}_x$, with the gradient of $\bar{F}$ defined as in (2.15), but with an additional integration over an x-interval, it follows that

$$\nabla\bar{S}(\boldsymbol{Z}) = k\nabla\bar{F}(\boldsymbol{Z}). \tag{3.2}$$

Periodic travelling waves are then 2π-periodic solutions of (3.2). Restricting the functional $\bar{F}$ to 2π-periodic functions and defining

$$\tilde{F} = \frac{1}{2\pi}\int_0^{2\pi} \bar{F}\,\mathrm{d}x,$$

we can characterize periodic travelling waves as critical points of $\bar{S}$ (recall that $\bar{S}$ is a spatial invariant and does not have to be averaged) on level sets of $\tilde{F}$, or, with $k \in \mathbb{R}$ as Lagrange multiplier, critical points of the unconstrained functional

$$\mathscr{F} = \bar{S} - k\tilde{F}, \tag{3.3}$$

since $\nabla\mathscr{F} = 0$ recovers (3.2). In the above variational principle a solution of $\nabla\mathscr{F} = 0$ depends on k. The integrals $\bar{S}$ and $\tilde{F}$ evaluated on a solution depend on k through $\boldsymbol{Z}$. Therefore

$$\partial_k \bar{S} = \langle \nabla\bar{S}(\boldsymbol{Z}), \boldsymbol{Z}_k \rangle = k\langle \nabla\tilde{F}(\boldsymbol{Z}), \boldsymbol{Z}_k \rangle = k\,\partial_k \tilde{F}.$$

It follows that $\partial_k \bar{S} = 0$ implies $\partial_k \tilde{F} = 0$ when $k \neq 0$. This property will be important in the analysis in §4.

In this section we will use the above variational principle to construct weakly nonlinear waves near (k_0, c_0). We expand the solution in a Fourier series in x;

$$\left.\begin{aligned} \eta(x) &= A_1 \cos x + A_2 \cos 2x + A_3 \cos 3x + \dots, \\ \phi(x,y) &= B_1 \mathrm{e}^{+ky} \sin x + B_2 \mathrm{e}^{+2ky} \sin 2x + B_3 \mathrm{e}^{+3ky} \sin 3x + \dots, \\ \phi'(x,y) &= B_1' \mathrm{e}^{-ky} \sin x + B_2' \mathrm{e}^{-2ky} \sin 2x + B_3' \mathrm{e}^{-3ky} \sin 3x + \dots. \end{aligned}\right\} \tag{3.4}$$

Expressions for the other components of $\boldsymbol{Z}$ (namely Φ, Φ', w, u and u') are easily obtained from (3.4) using the definitions in (2.5)–(2.7). Substitution of (3.4) into (3.3) results in

$$\mathscr{F} = \mathscr{F}(A_1, A_2, \dots, B_1, B_2, \dots, B_1', B_2', \dots; k).$$

Retaining three coefficients in the expansions and setting $\partial\mathscr{F}/\partial B_j = \partial\mathscr{F}/\partial B_j' = 0$ for $j = 1, 2, 3$ and $\partial\mathscr{F}/\partial A_j = 0$ for $j = 2, 3$ yields the following expressions for the coefficients:

$$\left.\begin{aligned} B_1 &= cA_1\{1 - \tfrac{3}{2}kA_2 + \tfrac{1}{8}k^2A_1^2\} - \tfrac{5}{2}ckA_2A_3 \\ &\quad + cA_1\{\tfrac{9}{8}k^2A_1A_3 + \tfrac{3}{4}k^2A_2^2 + \tfrac{5}{24}k^3A_2A_1^2 + \tfrac{3}{64}k^4A_1^4\} + \dots, \\ B_2 &= c\{A_2 - \tfrac{1}{2}kA_1^2 + A_1[-2kA_3 + \tfrac{3}{2}k^2A_2A_1 - \tfrac{5}{24}k^3A_1^3]\} + \dots, \\ B_3 &= c\{A_3 - \tfrac{3}{2}kA_1A_2 + \tfrac{3}{8}k^2A_1^3\} + \dots, \end{aligned}\right\} \tag{3.5}$$

$$\left.\begin{aligned} B_1' &= -cA_1\{1 + \tfrac{3}{2}kA_2 + \tfrac{1}{8}k^2A_1^2\} - \tfrac{5}{2}ckA_2A_3 \\ &\quad - cA_1\{\tfrac{9}{8}k^2A_1A_3 + \tfrac{3}{4}k^2A_2^2 - \tfrac{5}{24}k^3A_2A_1^2 + \tfrac{3}{64}k^4A_1^4\} + \dots, \\ B_2' &= -c\{A_2 + \tfrac{1}{2}kA_1^2 + A_1[2kA_3 + \tfrac{3}{2}k^2A_2A_1 + \tfrac{5}{24}k^3A_1^3]\} + \dots, \\ B_3' &= -c\{A_3 + \tfrac{3}{2}kA_1A_2 + \tfrac{3}{8}k^2A_1^3\} + \dots, \end{aligned}\right\} \tag{3.6}$$

and

$$A_2 = g_1A_1^2 + g_2A_1^4 + \dots, \quad A_3 = g_3A_1^3 + \dots, \tag{3.7}$$

where

$$\left.\begin{aligned} g_1 &= \tfrac{1}{2}(k^2/\beta_2)(\rho - \rho')c^2, \\ g_2 &= (g_1/\beta_2)\{2\beta_2(2g_3 - \tfrac{7}{24}k^2) - 3\sigma k^4 + \tfrac{3}{2}k^3(\rho + \rho')c^2\}, \\ g_3 &= \tfrac{1}{2}(k^4/\beta_3)\{\tfrac{3}{4}\sigma - (\rho - \rho')c^2/2k + (2/\beta_2)(\rho - \rho')^2c^4\}, \end{aligned}\right\} \tag{3.8}$$

with

$$\beta_n = (\rho + \rho')nkc^2 - (\rho - \rho')g - \sigma n^2k^2.$$

Substitution of (3.5)–(3.7) into the expression for $\mathscr{F}$ results in a reduced functional $\tilde{\mathscr{F}}(A_1; k; p)$ where p indicates parameters. Setting $\partial\tilde{\mathscr{F}}/\partial A_1 = 0$ results in the bifurcation equation for the travelling waves, which, accurate to fifth order, is

$$A_1 f(z, k, c, r) = 0,$$

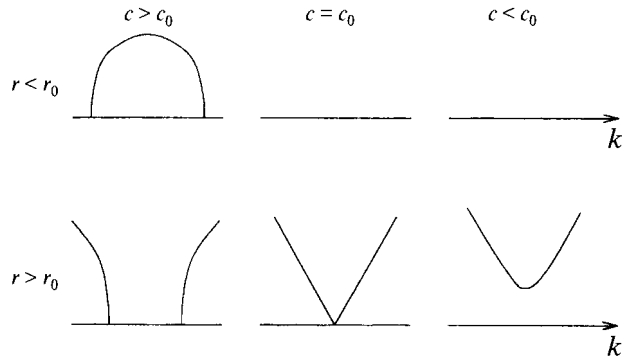

FIGURE 5. Bifurcation of travelling waves near the critical point (k_0, c_0) when $r \neq r_0$.

with $$f = (\rho+\rho')c^2k-(\rho-\rho')g-\sigma\kappa^2+f_1 z+f_2 z^2+\ldots. \tag{3.9}$$

The definitions of the new symbols are

$$z = A_1^2,$$

$$f_1 = -\tfrac{1}{2}k^4\left[(\rho+\rho')\frac{c^2}{k}-\tfrac{3}{4}\sigma+\frac{(\rho-\rho')^2c^4}{\beta_2}\right],$$

$$f_2 = -\tfrac{15}{64}\sigma k^6+\tfrac{11}{32}(\rho+\rho')c^2k^5+\tfrac{7}{4}k^4(\rho-\rho')c^2g_1-3\beta_3 g_3^2-\tfrac{9}{2}k^3g_1^2[(\rho+\rho')c^2-2\sigma k].$$

Let us first consider the bifurcations in the neighbourhood of the critical point $(0, k_0, c_0, r)$ (the minimum of the dispersion curve) away from the singularity $r = r_0$, which corresponds to the vanishing of f_1. Recall that

$$k_0 = [(\rho-\rho')g/\sigma]^{1/2} = [2r\rho g/(1+r)\sigma]^{1/2},$$
$$c_0 = [2\sigma k_0/(\rho+\rho')]^{1/2} = [\sigma k_0(1+r)/\rho].^{1/2}$$

The simplest Taylor expansion of f about that critical point yields

$$f = -\sigma(k-k_0)^2+\frac{4}{c_0}\sigma k_0^2(c-c_0)+2\sigma k_0^4(r^2-r_0^2)z+\ldots.$$

The corresponding bifurcation diagrams are as shown in figure 5 and they verify the diagrams presented in figure 1(*b*, *c*). The bifurcation of periodic travelling waves is analogous to the bifurcation that occurs in the unfolding of the collision of eigenvalues of opposite signature in a finite-dimensional Hamiltonian system (compare with figure 2 of Bridges 1990). The diagrams are also reminiscent of the bifurcation diagrams near the Kelvin–Helmholtz instability (compare with figure 3.1 of Benjamin & Bridges 1992, part II) but in the Kelvin–Helmholtz problem c is the abscissa and $U-U'$ is the control parameter.

In the neighbourhood of $r = r_0(=\frac{1}{4}\sqrt{5})$ the bifurcations of travelling waves become more complex. The coefficient of z in f vanishes and higher-order terms are needed. Note that the singularity $r = r_0$ corresponds to the singularity $\alpha+\beta = 0$ in Dias & Bridges (1994) (fixing $b = 1$ along the curve between regions 4 and 5 in figure 5.1 of Dias & Bridges, which corresponds to the minimum of the dispersion curve). The simplest Taylor expansion of f about the point $(0, k_0, c_0, r_0)$ is

$$f = -\sigma(k-k_0)^2+(4/c_0)\sigma k_0^2(c-c_0)+f^0_{rz}(r-r_0)z+f^0_{kz}(k-k_0)z+\tfrac{1}{2}f^0_{zz}z^2+\ldots, \tag{3.10}$$

where the superscript 0 denotes evaluation at the critical point. One easily finds that

$$f^0_{rz} = 4r_0\sigma k_0^4 > 0, \quad f^0_{kz} = -\tfrac{3}{2}\sigma k_0^3 < 0, \quad f^0_{zz} = \tfrac{1}{128}\sigma k_0^6(21\sqrt{5}-1) > 0.$$

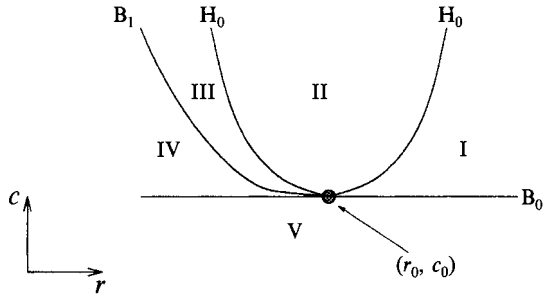

FIGURE 6. Partition of the (r, c)-plane near (r_0, c_0) into regions with distinct bifurcation diagrams.

Introducing the following scaling of the variables:

$$\tilde{z} = z(\tfrac{1}{2}f^0_{zz})^{1/2}, \quad \tilde{k}-\tilde{k}_0 = (k-k_0)\,\sigma^{1/2},$$

$$\tilde{c}-\tilde{c}_0 = \frac{4\sigma k_0^2}{c_0}(c-c_0), \quad \tilde{r}-\tilde{r}_0 = \frac{f^0_{rz}(r-r_0)}{(2f^0_{zz})^{1/2}},$$

(3.10) becomes

$$f = -(\tilde{k}-\tilde{k}_0)^2+(\tilde{c}-\tilde{c}_0)+2(\tilde{r}-\tilde{r}_0)\,\tilde{z}-\frac{\sqrt{2}|f^0_{kz}|}{(\sigma f^0_{zz})^{1/2}}(\tilde{k}-\tilde{k}_0)\,\tilde{z}+\tilde{z}^2+\ldots.$$

Letting

$$m = \frac{|f^0_{kz}|}{(2\sigma f^0_{zz})^{1/2}} = \frac{12}{(21\sqrt{5}-1)^{1/2}}, \tag{3.11}$$

the basic (truncated) equation for bifurcating travelling waves near the codimension-2 point (r_0, c_0) is

$$f = -(\tilde{k}-\tilde{k}_0)^2+(\tilde{c}-\tilde{c}_0)+2(\tilde{r}-\tilde{r}_0)\,\tilde{z}-2m(\tilde{k}-\tilde{k}_0)\,\tilde{z}+\tilde{z}^2. \tag{3.12}$$

The solutions set of this type of equation has been analysed completely by Golubitsky & Schaeffer (1985, pp. 272–278) and by Bridges (1990, pp. 591–595). The solution set can be quite complicated and depends on the region in the (c, r)-space. Using the theory in the aforementioned references the (c, r)-plane is divided into regions as shown in figure 6, each region having a distinct bifurcation diagram as shown in figure 7.

In figure 7 the wavenumber versus amplitude is plotted. For c fixed and $c > 0$ the bifurcation diagrams depend on r. For $r \ll r_0$ the only branch for sufficiently small amplitude is the globally connected branch (as expected from figure 5). But as r is increased to region IV an additional disconnected branch appears (for a given wavenumber there are two branches of travelling waves with that wavenumber but with differing amplitudes). Along B_1 the isolated branch forms a bifurcation point with the loop resulting in two branches which then break apart when r is increased beyond the values corresponding to B_1. Further increase in the value of r leads to region I which is qualitatively similar then for all $r \gg r_0$ (in agreement with figure 5).

Along the curve B_1 the two branches of travelling waves exactly intersect as shown in figure 7 (diagram B_1). The B_1 curve in the (c, r)-plane is a half-parabola defined by $f = f_z = f_k = 0$ which results in

$$\frac{c-c_0}{c_0} = \frac{5}{9}\left(\frac{m^2}{m^2+1}\right)(r-r_0)^2 \quad \text{with} \quad r-r_0 < 0.$$

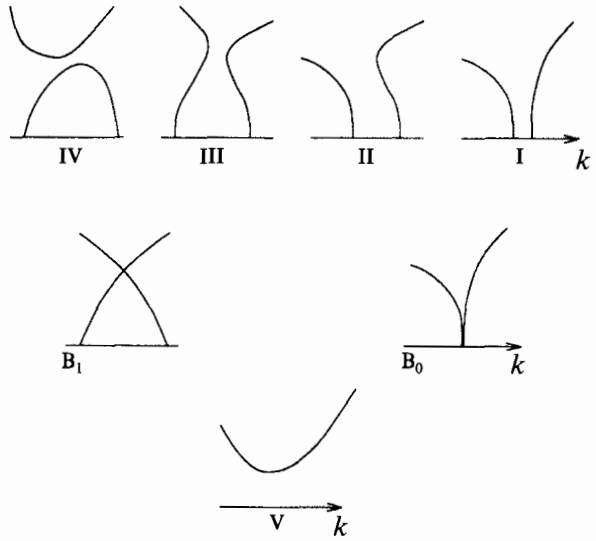

FIGURE 7. Qualitative bifurcation diagrams for travelling waves near the critical point (k_0, c_0, r_0) labelled by region number as in figure 6.

Similarly, along the curve H_0 in the (c, r)-plane a branch changes bifurcation direction. The curve H_0 is a parabola defined by $f = f_z = 0$ (and $z = 0$) which results in

$$\frac{c-c_0}{c_0} = \tfrac{5}{9}(r-r_0)^2.$$

Note that the curves B_1 and H_0 are parabolas in the neighbourhood of (r_0, c_0) in the (r, c) plane. However, these curves have some global (that is for (r, c) far from (r_0, c_0)) continuation that could be followed numerically.

4. Spatial invariants and secondary bifurcations

The spatial Hamiltonian structure points to the importance of the functionals $\bar{S}$, $\bar{Q}$, $\bar{Q}'$ and $\bar{F}$. Evaluation of these integrals along branches of travelling waves leads to interesting geometrical information. It turns out that the slopes of the curves in parameter space carry information about secondary bifurcation of waves. In this section the theory of Saffman (1985) for the superharmonic instability will be adapted to the spatial setting to obtain the results on the movement of spatial Floquet multipliers.

To evaluate the integrals the results of §3 for travelling waves near the singularity $c = c_g$ are used, concentrating on the cases $r \neq r_0$ and $r < r_0$. Further bifurcations occur when $r \approx r_0$ and the integrals in this case will be evaluated numerically in §5.

Evaluating $\bar{F}$ at a periodic travelling wave and averaging over a wavelength results in

$$\bar{F} = \tfrac{1}{2}\sigma(k-k_0)A_1^2 - \sigma\frac{k_0}{c_0}(c-c_0)A_1^2 + \tfrac{3}{16}\sigma k_0^3 A_1^4 + \dots. \tag{4.1}$$

A similar calculation for $\bar{S}, \bar{Q}$ and $\bar{Q}'$ results in

$$\left.\begin{aligned} \bar{S} &= \tfrac{1}{4}\sigma(k^2-k_0^2)A_1^2 + \tfrac{1}{4}\sigma k_0^4(r^2+\tfrac{7}{16})A_1^4 + \dots, \\ \bar{Q} &= \tfrac{1}{2}\rho c k A_1^2 + \tfrac{1}{2}\rho c k^3(2r^2+r-\tfrac{1}{4})A_1^4 + \dots, \\ \bar{Q}' &= \tfrac{1}{2}\rho' c k A_1^2 + \tfrac{1}{2}\rho' c k^3(2r^2-r-\tfrac{1}{4})A_1^4 + \dots, \end{aligned}\right\} \tag{4.2}$$

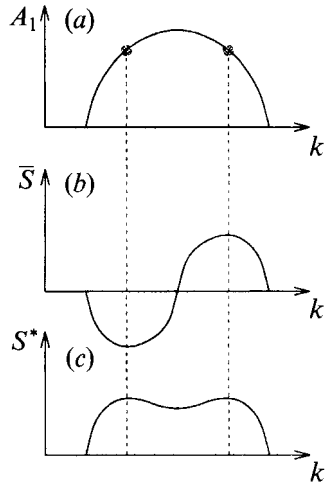

FIGURE 8. Amplitude, $\bar{S}$ and S^* as functions of wavenumber k for branching travelling waves when $r < r_0$ and $c > c_0$.

and therefore

$$\bar{Q}_{tot} = \bar{Q} + \bar{Q}' = \tfrac{1}{2}(\rho+\rho')\, ckA_1^2 + \tfrac{1}{2}(\rho+\rho')\, ck^3(3r^2 - \tfrac{1}{4})\, A_1^4 + \ldots .$$

For fixed c and r each of the above expressions depends only on the wavenumber k through the bifurcation equation

$$\sigma(k-k_0)^2 - (4/c_0)\,\sigma k_0^2(c-c_0) - 2\sigma k_0^4(r^2-r_0^2)\, A_1^2 + \ldots = 0. \tag{4.3}$$

A shifted flow force is defined by

$$S^* \overset{\text{def}}{=} \bar{S} - k_0\tilde{F} = \tfrac{1}{4}\sigma(k-k_0)^2 A_1^2 + \sigma\frac{k_0^2}{c_0}(c-c_0)\, A_1^2 + \tfrac{1}{4}\sigma k_0^4(r^2-r_0^2)\, A_1^4 + \ldots$$

$$= \tfrac{1}{8}[3\sigma(k-k_0)^2 + 4\sigma\frac{k_0^2}{c_0}(c-c_0)]\, A_1^2 + \ldots .$$

Figure 8 shows the integrals $\bar{S}$ and S^* plotted as a function of k. First, in (*a*) the amplitude as a function of wavenumber is plotted using (4.3). The branch of travelling waves is globally connected when plotted as a function of wavenumber. There are two points along the branch that are important for secondary bifurcations but the amplitude versus wavenumber diagram does not show these points (although they are marked for reference to the other figures). In figure 8(*b*) the flow force, using (4.2), is plotted versus wavenumber. Note that there are two points where $\partial_k \bar{S} = 0$. In figure 8(*c*) the rotated flow force S^* is plotted. Maxima of S^* correspond to points where $\partial_k \bar{S} = 0$. In § 5 more complete results on the waves in invariant space are given and $\bar{Q}_{tot}$ along the branches of travelling waves is also plotted.

As noted in the introduction, when $\bar{S}$, the flow force, is plotted versus $\tilde{F}$, the spatial action, cusp points appear when $\partial_k \bar{S} = 0$. Moreover, the travelling waves in $(S^*, \tilde{F})$-space form the boundary of a swallowtail. This is verified as follows. Introduce scaled variables

$$\lambda = k/k_0 - 1 \quad \text{and} \quad \mu = (4/c_0)(c-c_0).$$

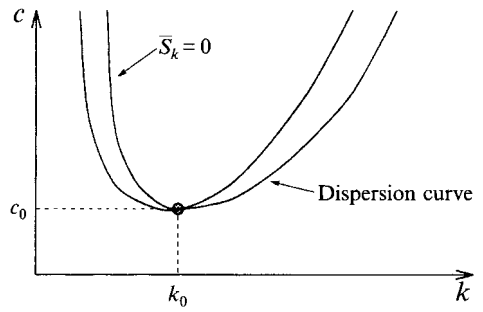

FIGURE 9. Projection of $\partial_k \bar{S} = 0$ curve onto the (k, c)-plane showing the region, between the two parabolas, where a pair of spatial Floquet multipliers lies on the unit circle.

Then, for μ and λ small the functionals $(S^*, \tilde{F})$ are

$$\tilde{F} = \left[\frac{\sigma}{4k_0(r_0^2 - r^2)}\right]\lambda(\mu - \lambda^2) + \ldots, \quad S^* = \left[\frac{\sigma}{16(r_0^2 - r^2)}\right](\mu + 3\lambda^2)(\mu - \lambda^2) + \ldots, \quad (4.4)$$

where A_1^2 has been eliminated using (4.3).

In (4.4) σ, k_0 and r are fixed. Moreover for any fixed $\mu > 0$ with μ sufficiently small (4.4) is the parametrization by λ of a curve in the $(S^*, \tilde{F})$-plane. It is straightforward to verify that the curve for $-\mu^{1/2} < \lambda < \mu^{1/2}$ forms the boundary of a swallowtail as shown in figure 2. The cusp points occur when $\mathrm{d}\tilde{F}/\mathrm{d}\lambda = \mathrm{d}S^*/\mathrm{d}\lambda = 0$ which results in $\lambda = \pm(\mu/3)^{1/2}$. Expressed in terms of c and k the cusp points satisfy, to leading order ($|c - c_0|, |k - k_0|$ small),

$$\frac{c - c_0}{c_0} = \frac{3}{4k_0^2}(k - k_0)^2 + \ldots, \quad (4.5)$$

which is a parabola in the (k, c)-plane, as shown in figure 9. On the other hand, the dispersion curve near (k_0, c_0) has the form

$$\frac{c - c_0}{c_0} = \frac{1}{4k_0^2}(k - k_0)^2 + \ldots$$

and therefore the projection of (4.5) onto the (k, c)-plane lies interior to the dispersion curve. We will argue that the curve (4.5) separates the region interior to the dispersion curve into two regions each containing distinctly different secondary bifurcations. To show this the theory of Saffman for superharmonic instability will be adapted to the spatial setting.

It is important to note in the following discussion the distinction between the use of Floquet theory in space and time. Whereas a hyperbolic Floquet multiplier in time corresponds to a linear instability, a hyperbolic Floquet multiplier in space does not in general have any significance for the linear stability in the time-dependent problem although it is possible to establish a relation in some cases (cf. Bridges 1992*a*, §5).

The theory of Saffman (1985) for the superharmonic instability can be summarized as follows. Consider the following Hamiltonian system

$$U_t = \boldsymbol{J}\nabla\mathscr{H}(U), \quad (4.6)$$

where for simplicity $U \in \mathbb{R}^{2n}$ (a finite dimensional approximation to the water-wave problem for example) and $\boldsymbol{J}$ is a constant skew-symmetric operator (constancy of $\boldsymbol{J}$ is not essential but simplifies the exposition). Suppose there exists a periodic solution of (4.6):

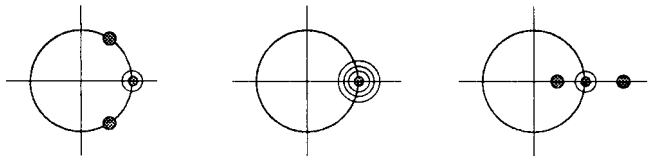

FIGURE 10. Position of Floquet multipliers predicted by the superharmonic instability theory.

$$U(t+2\pi/\omega) = U(t)$$

with ω, the frequency, varying along a branch of periodic states. Now consider the linearization of (4.6) about the periodic state

$$\hat{U}_t = \boldsymbol{J} D^2 \mathscr{H}(U)\, \hat{U}. \tag{4.7}$$

It is clear that $\hat{U} = U_t$ is always a solution of (4.7). Therefore zero is a Floquet exponent of (4.6) (it is in fact double: algebraic multiplicity two but geometric multiplicity one). Saffman's theorem states that a necessary condition for a quadruple zero Floquet exponent (since zero eigenvalues always occur in pairs algebraic multiplicity three is not possible) is $d\mathscr{H}/d\omega = 0$. In other words the Hamiltonian function plotted versus the frequency along a branch should be stationary (in the water-wave problem the superharmonic instability corresponds to a maximum in $(\mathscr{H}, \omega)$-space). In Saffman's paper the argument is posed in terms of c, the wave speed; but since the wavenumber is fixed there the argument is equivalent to that with the frequency. The movement of Floquet multipliers is as shown in figure 10 (the theory predicts only the middle picture but under generic perturbation the eigenvalues move as shown in the adjacent pictures). The theory does not predict whether $d\mathscr{H}/d\omega$ positive or negative correspond to the stable case; only that there is a change of stability when $d\mathscr{H}/d\omega = 0$. Therefore we introduce an application-dependent parameter $\epsilon = \pm 1$. For example $\epsilon = +1$ for the superharmonic instability that occurs in the water-wave problem (that is, when $d\mathscr{H}/d\omega > 0$ the wave is superharmonic-stable). Another feature of the superharmonic instability theory is that the frequency (or wave speed if k is fixed) and the Hamiltonian function have maxima at different values of the amplitude, in general.

It is interesting to note that, for finite-dimensional Hamiltonian systems, the connection between stationary points of the Hamiltonian function, along branches of periodic orbits, when plotted as a function of the frequency, and the movement of Floquet multipliers is a standard tool in the numerical calculation of branches of periodic orbits in celestial mechanics (cf. Deprit & Henrard 1968).

The superharmonic instability has an analogue in the spatial setting. The analogous Hamiltonian functional in (4.6) is the flow force, the action is the functional $\bar{F}$ and the analogue of the frequency is the wavenumber, since in the spatial setting the wavenumber is taken to vary along the branch of waves. In fact figure 8 presents precisely the features of the superharmonic instability in space (although no instability is implied in the spatial setting); $dA_1/dk = 0$ at a different point from that where $\partial_k \bar{S} = 0$ ($\partial_k \bar{S}$ is the analogue of $d\mathscr{H}/d\omega$) and moreover it is an immediate consequence of Saffman's theory that when $\partial_k \bar{S} = 0$ *a* spatial Floquet multiplier is entering or leaving the unit circle through $+1$ as shown in figure 10 (with $(\mathscr{H}, \omega)$ replaced by $(\bar{S}, k)$).

Since $\partial_k \bar{S} = 0$ twice in the interval in which the global loop of travelling waves exists

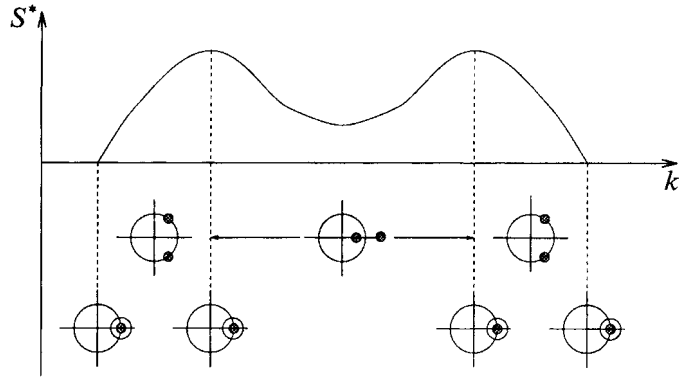

FIGURE 11. Position of spatial Floquet multipliers treated as a function of S^* and wavenumber k.

in figure 8 the movement of the spatial Floquet multipliers is as shown in figure 11. It is remarkable that such bifurcations of the spatial Floquet multipliers occur at low amplitude. For example such bifurcations have been found numerically at large amplitude in the classic water-wave problem by Baesens & MacKay (1992) and in a modified Korteweg–de Vries equation by Zufiria (1987). In Bridges (1992*a*) a model problem with spatial collision of multipliers and a swallowtail in invariant space is studied (see §4 of Bridges (1992*a*) particularly figures 2, 6, 8 and 9). From a theoretical point of view, the present results show that capillary–gravity interfacial waves have the advantage that interesting secondary bifurcations occur at low amplitude and can therefore be studied analytically.

There are two distinct regions along the branch separated by the points where $\partial_k \bar{S} = 0$. In the region between the two parabolas in figure 9, where $\partial_k \bar{S} < 0$, the second pair of multipliers on the unit circle would lead to bifurcations of p/q subharmonics as in Longuet-Higgins (1985) and Baesens & MacKay (1992). However, in the interior range (in terms of (μ, λ) coordinates: $-(\mu/3)^{1/2} < \lambda < (\mu/3)^{1/2}$) the basic pair of Floquet exponents is hyperbolic. The hyperbolic periodic states have a stable and unstable manifold. If the stable and unstable manifolds should intersect then the resulting state could be a solitary wave. In fact, inspired by the present analysis, the region where the spatial Floquet multipliers are hyperbolic has been analysed by Dias & Iooss (1994) and they have shown that indeed a new family of solitary waves exist along this branch. They are 'dark' solitary waves (using terminology from optics theory); they are biasymptotic to periodic states as $x \to \pm\infty$ whose amplitude does not decay to zero.

5. Finite-amplitude travelling waves – numerical computations

Our aim in this section is to study numerically the bifurcations of finite-amplitude interfacial travelling waves near the critical point (k_0, c_0) in general and near the point (k_0, c_0, r_0) in particular. For the numerical computations we use a scheme, based on a Fourier collocation method, originally proposed by Saffman & Yuen (1982) for computing interfacial gravity waves in the presence of a current and modified by Bontozoglou & Hanratty (1990) for interfacial capillary–gravity waves. It is customary in the numerical computation of water waves to fix the wavenumber k and solve for the wave speed c along a branch of travelling waves. A key feature of the present work is the importance of the dependence of the solution branches on the wavenumber, with

c treated as a control parameter. It is precisely the variation of the wavenumber along solution branches that leads to the spatial bifurcations studied here. The spatial bifurcations near the codimension-2 point (c_0, r_0) and the bifurcations in invariant spaces $(\bar{F}, \bar{S})$ and $(\bar{Q}_{tot}, \bar{S})$ are considered numerically.

Using an inverse formulation the physical coordinates (x, y) below and (x', y') above the interface are expanded in finite Fourier series in the complex potentials $\phi + i\psi$ for the lower fluid and $\phi' + i\psi'$ for the upper fluid:

$$\begin{pmatrix} x \\ y \end{pmatrix} = \frac{1}{ck}\begin{pmatrix} \phi \\ \psi \end{pmatrix} + \frac{1}{k}\begin{pmatrix} 0 \\ a_0 \end{pmatrix} + \frac{1}{k}\sum_{n=1}^{N} a_n \begin{pmatrix} \sin(n\phi/kc) \\ \cos(n\phi/kc) \end{pmatrix} e^{n\psi/kc}, \tag{5.1}$$

$$\begin{pmatrix} x' \\ y' \end{pmatrix} = \frac{1}{ck}\begin{pmatrix} \phi' \\ \psi' \end{pmatrix} + \frac{1}{k}\begin{pmatrix} 0 \\ a_0' \end{pmatrix} + \frac{1}{k}\sum_{n=1}^{N} a_n' \begin{pmatrix} \sin(n\phi'/kc) \\ -\cos(n\phi'/kc) \end{pmatrix} e^{-n\psi'/kc}. \tag{5.2}$$

Without loss of generality ψ and ψ' are defined so that they are equal to zero on the interface.

Details on how to compute the unknowns $a_0, a_1, \ldots, a_N, a_0', a_1', \ldots, a_N', s_2, \ldots, s_N$ (where N is the truncation order) can be found in the references mentioned at the beginning of the section. For the numerical computations a scaling such that $g = \sigma = \rho = 1$ is chosen. In all the computations presented below, forty mesh points ($N = 40$) were used, a number that was found sufficient to ensure accuracy for computing waves of small energy.

To obtain expressions for the kinetic and potential energies we integrate and average the expressions for K, V_g and V_σ in Appendix A, equation (A 4). This results in

$$\hat{K} = \frac{k}{\pi}\int_0^{\pi/k} K\,dx = \tfrac{1}{2}c^2\left[\left(\frac{1-r}{1+r}\right)a_0' - a_0\right],$$

$$\hat{V}_g = \frac{k}{\pi}\int_0^{\pi/k} V_g\,dx = \frac{k}{\pi}\frac{r}{1+r}\int_0^{\pi/k} \eta^2(\xi)\frac{dx}{d\xi}d\xi,$$

$$\hat{V}_\sigma = \frac{k}{\pi}\int_0^{\pi/k} V_\sigma\,dx = \frac{k}{\pi}\int_0^{\pi/k} [(1+(\eta_\xi/x_\xi)^2)^{1/2} - 1]\frac{dx}{d\xi}d\xi.$$

The spatial Hamiltonian structure points to the importance of the functionals $\bar{S}$, $\tilde{F}$ and $\bar{Q}_{tot}$. These functionals can be expressed in terms of the averaged energies (see Appendix A). A summary is given in the form

$$\begin{pmatrix} \bar{Q}_{tot} \\ \tilde{F} \\ \bar{S} \end{pmatrix} = \begin{bmatrix} 2/c & 0 & 0 \\ 1 & -2 & 0 \\ 2 & -3 & -1 \end{bmatrix} \begin{pmatrix} \hat{K} \\ \hat{V}_g \\ \hat{V}_\sigma \end{pmatrix}.$$

We begin with the case where r is close to one (small upper fluid density) and as expected the results are similar to the results of the basic water-wave problem. Figure 12(a–c) shows the bifurcation diagrams for $r = 0.9$ in three different planes, with c treated as control parameter. The wavenumber–amplitude diagrams in figure 12(a) are in qualitative agreement with those in figure 5. Starting with $c > c_0$, the two branches of travelling waves (the capillary branch and the gravity branch) meet at $(k_0, 0)$ for $c = c_0$ and then, for $c < c_0$, they detach as a single branch. Note that in the numerically computed pictures there is a decrease in the slope of the 'left' branch when k is smaller

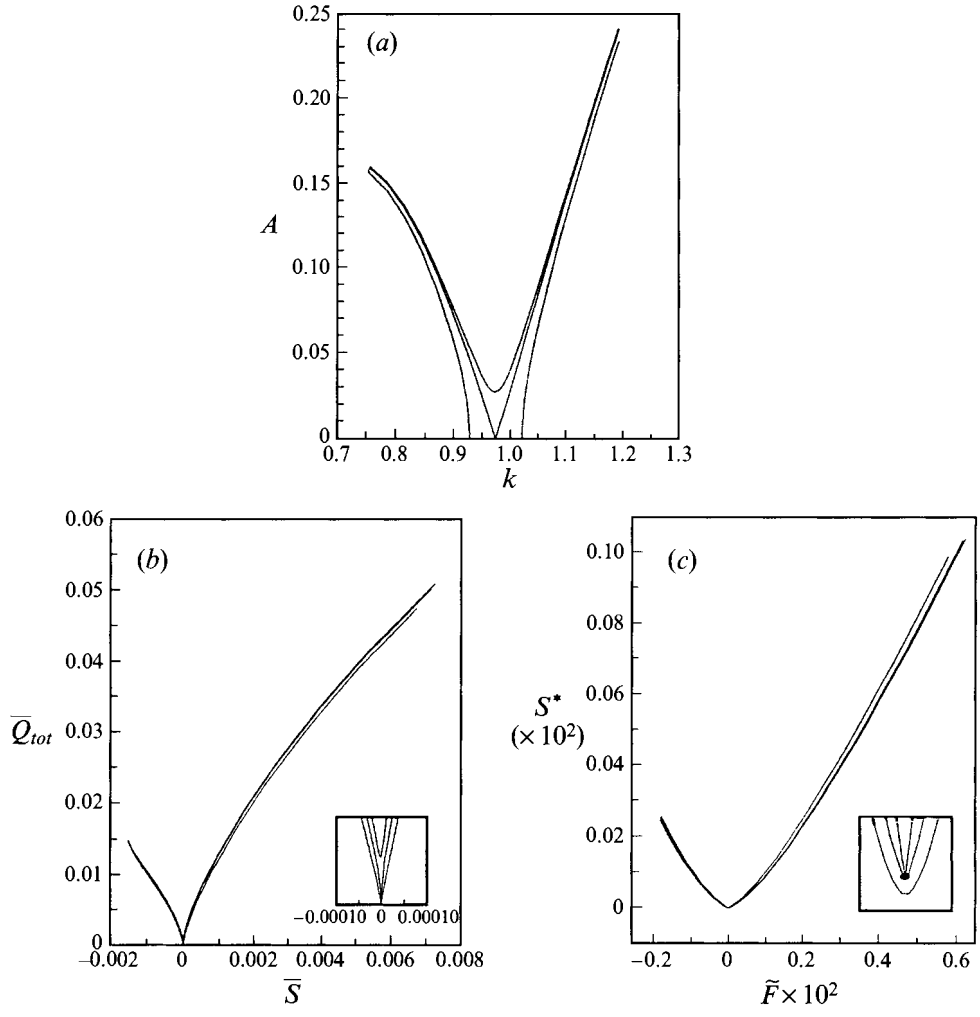

FIGURE 12. Numerical branches of travelling waves in three different planes for $r = 0.9$. (*a*) (k, A)-plane. The outer branches correspond to $c > c_0$, the middle one to $c = c_0$ and the inner (detached) one to $c < c_0$. (*b*) $(\bar{S}, \bar{Q}_{tot})$-plane: same as in (*a*), with three branches hard to distinguish. The blow-up near the origin (inset) provides a better visualization. (*c*) $(\tilde{F}, S^*)$-plane: the inner branch corresponds to $c > c_0$, the middle one to $c = c_0$ and the outer one to $c < c_0$. Again a blow-up near the origin allows a better visualization.

than a critical (parameter-dependent) value. This is due to the 1:2 resonance phenomenon occurring in the neighbourhood of $k = 1/\sqrt{2}$. The diagrams in the $(\bar{Q}_{tot}, \bar{S})$-plane in figure 12(*b*) behave as in the basic water-wave problem (Bridges 1992*b*, figure 5). In the $(\tilde{F}, S^*)$-plane (see figure 12*c*), the branches of travelling waves are of opposite curvature to the ones in the $(\bar{Q}_{tot}, \bar{S})$-plane and the detached branch takes negative values near the origin.

In figure 13(*a–c*), the other extreme for the parameter r is illustrated. When $c \leqslant c_0$ there are no solutions at low amplitude. When $c > c_0$ we find numerically a globally connected branch of travelling waves in agreement with the theory in §3. This is shown in figure 13(*a*) for $r = 0.1$. A plot of the branch in the $(\bar{Q}_{tot}, \bar{S})$-plane results in a balloon-shaped region. Considering that $\bar{Q}_{tot}$ and $\bar{S}$ are absolute spatial invariants, it is natural to ask what types of solutions correspond to the interior points in the balloon region

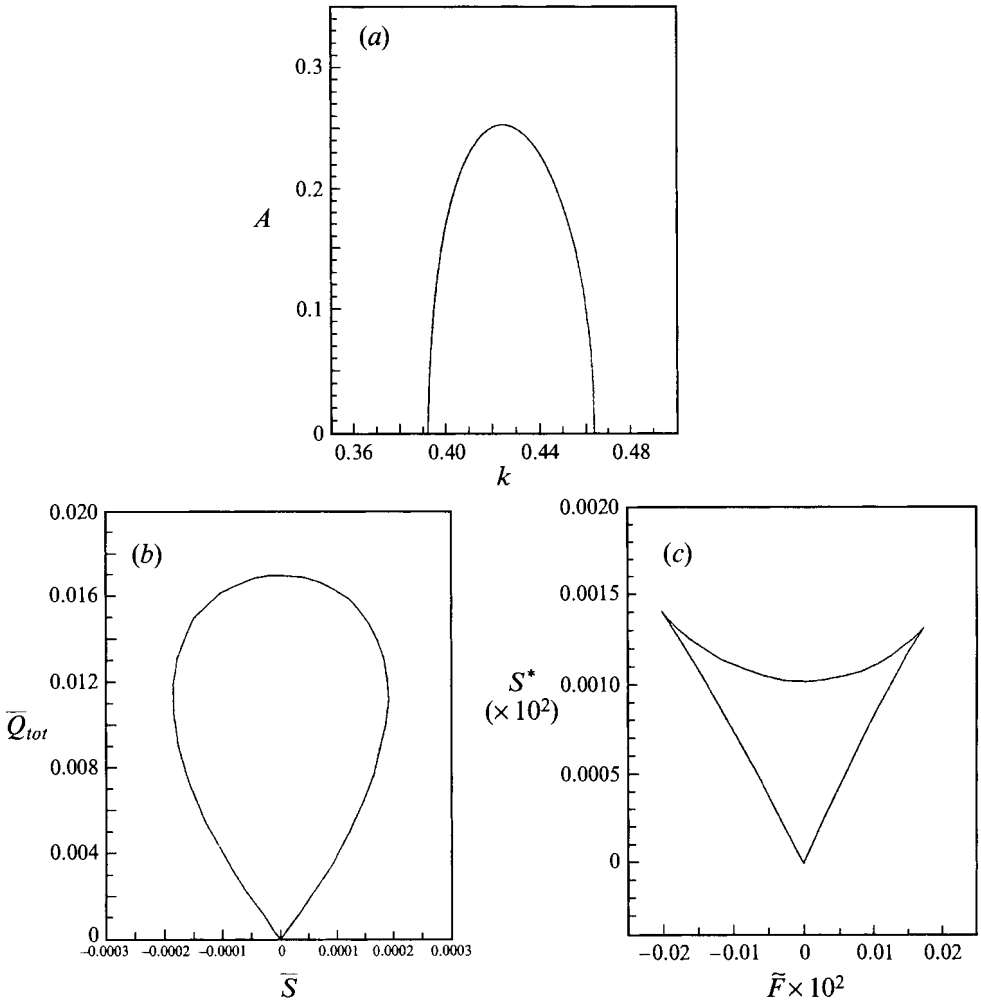

FIGURE 13. Numerical branches of travelling waves in three different planes as in figure 12 but for $r = 0.1$ and $c > c_0$.

in figure 13(*b*). A discussion will be provided in §7. In figure 13(*c*) the numerical results reveal the swallowtail in the $(\tilde{F}, S^*)$-plane, as predicted by the weakly nonlinear analysis.

Next we show results of numerical calculations for $|r - r_0|$ and $|c - c_0|$ small. In figures 14–16 the parameter r is equal to 0.53, which is slightly less than r_0, and c is varied from $c > c_0$ to $c < c_0$. Referring to figure 6 we will follow a vertical line in the (r, c)-plane to the left of the point (r_0, c_0), so that we pass from region II into region V through regions III and IV (region I is qualitatively similar to that for large r as shown in figure 12). For six different values of c, figures 14–16 show respectively the wavenumber–amplitude diagram, the $(\bar{Q}_{tot}, \bar{S})$-diagram and the $(\tilde{F}, S^*)$-diagram.

In figures 14(*a*) and 14(*b*), c is respectively in regions II and III of figure 6. The results agree qualitatively with the analytic predictions shown in figure 7. Lowering c further we meet the curve B_1 which indicates a bifurcation point and the numerical results capture this point perfectly as shown in figure 14(*c*). Lowering c further we find in figure 14(*d*) that the global loop and a disconnected branch are formed as the

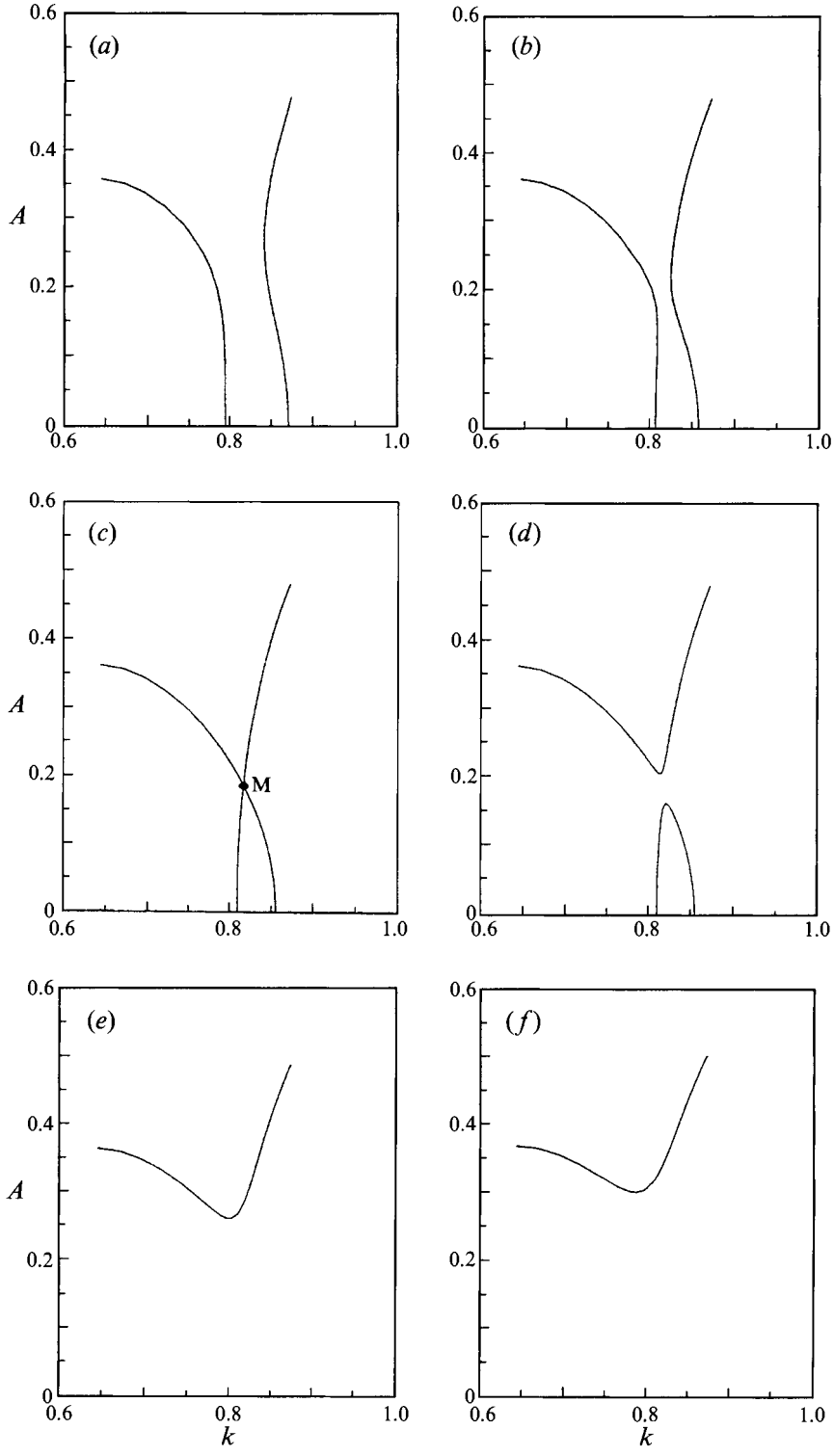

FIGURE 14. Numerical branches of travelling waves in the (k, A)-plane for $r = 0.53$ and six different values of c: (*a*) $c = 1.129083 > c_0$, (*b*) $c = 1.128754 > c_0$, (*c*) $c = 1.128710 > c_0$, (*d*) $c = 1.128699 > c_0$, (*e*) $c = 1.128494 = c_0$, (*f*) $= 1.128096 < c_0$.

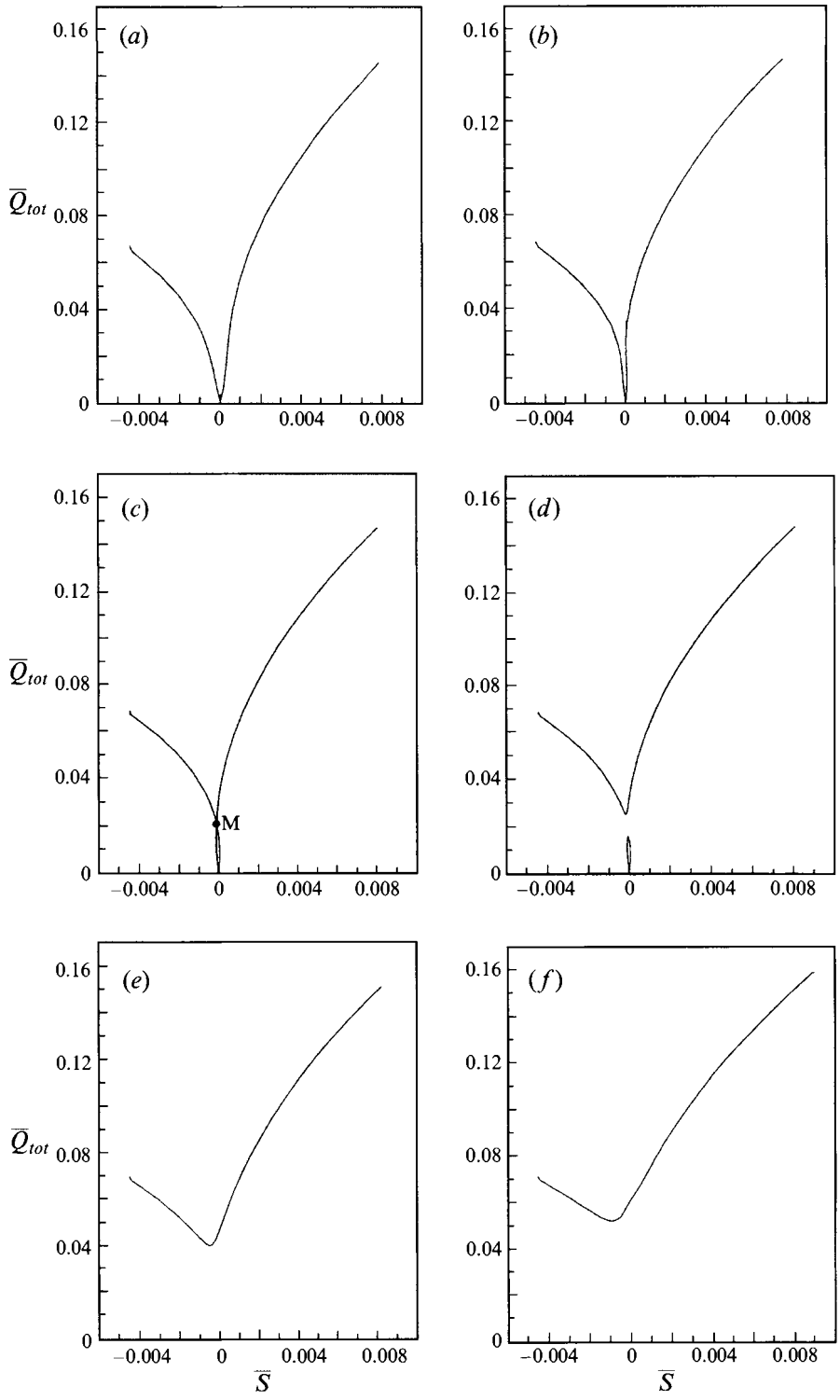

FIGURE 15. Same as figure 14 but in the $(\bar{S}, \bar{Q}_{tot})$-plane.

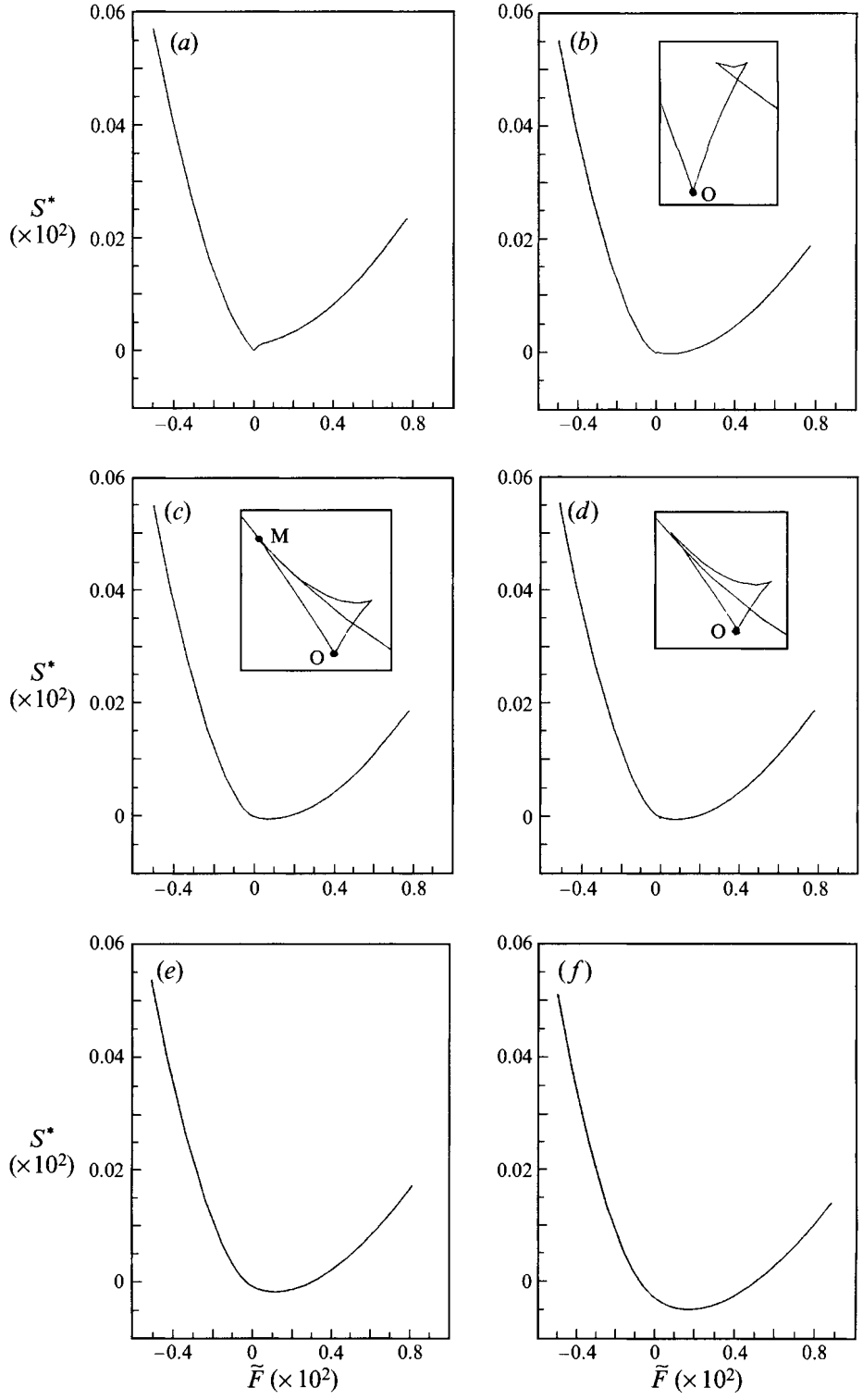

FIGURE 16. Same as figure 14 but in the $(\tilde{F}, S^*)$-plane. Blow-ups near the origin O where necessary allow for a better visualization.

bifurcation point breaks up as predicted analytically. When $c = c_0$, as shown in figure 14(*e*), the disconnected branch persists at finite amplitude and the global loop disappears. The numerical results then show in figure 14(*f*) that when c is in region V ($c < c_0$) the disconnected branch persists.

Next, we present the branches of travelling waves in the proper invariant spaces. Figure 15(*a–f*) shows the transition from $c > c_0$ to $c < c_0$ in the $(\bar{Q}_{tot}, \bar{S})$-plane, where the bifurcation points always lie at the origin. When $c < c_0$, the bifurcation point disappears but the detached branch persists even for values of c much smaller than c_0. The weakly nonlinear analysis pointed out the importance of the $(\tilde{F}, S^*)$-plane. This is confirmed by the numerical results. Figure 16(*a–f*) clearly shows the formation of the swallowtail that is present when r is less than r_0. In the present case (r just below r_0), the numerical results show that the swallowtail only exists for values of c just above c_0. In figure 16(*a–d*), c is above c_0. In figure 16(*a*), there is a sharp change in slope on the right-hand branch (the capillary branch) near the origin. As c is decreased, the capillary branch crosses itself and a small swallowtail with two cusps appears near the origin (see figure 16*b*). As c is decreased even further, the cusp point on the left moves towards the left-hand branch (the gravity branch). A second swallowtail appears along the gravity branch but almost immediately merges with the other swallowtail. This case, which is shown in figure 16(*c*), corresponds to the merging of the two branches of travelling waves which was already described in figure 14(*c*). This bifurcation point is denoted by M in all three planes. As one continues to decrease c, the detached branch moves down and the swallowtail corresponding to the globally connected branch shrinks. This is shown in figure 16(*d*). Finally, for $c = c_0$ the swallowtail disappears and for $c < c_0$ the remaining branch keeps moving downward (see figure 16*e*,*f*).

6. Analogy with the Kelvin–Helmholtz instability

There is an interesting mathematical analogy between the spatial bifurcations near the critical point at which $c = c_g$ and the temporal bifurcations near the Kelvin–Helmholtz instability. The Hamiltonian structure of the Kelvin–Helmholtz problem has recently been investigated by Benjamin & Bridges (1992). The basic Hamiltonian structure for the time-dependent problem can be seen by considering a single-mode approximation of the linear problem.

The interface boundary conditions for the linearized time-dependent problem are

$$\left.\begin{aligned} \eta_t + U\eta_x - \phi_y &= 0 \\ \eta_t + U'\eta_x - \phi'_y &= 0 \\ \rho(\phi_t + U\phi_x) - \rho'(\phi'_t + U'\phi'_x) + (\rho - \rho')\, g\eta - \sigma\eta_{xx} &= 0 \end{aligned}\right\} \quad \text{at} \quad y = 0. \tag{6.1}$$

A single-mode approximation for the linearized problem with infinite upper and lower layers is

$$\begin{aligned} \eta(x,t) &= q_1(t)\cos\kappa x + q_2(t)\sin kx, \\ \phi(x,t) &= \mathrm{e}^{ky}\,[e_1(t)\cos kx + f_1(t)\sin kx], \\ \phi'(x,t) &= \mathrm{e}^{-ky}\,[e'_1(t)\cos kx + f'_1(t)\sin kx]. \end{aligned}$$

The functions $\phi(\phi')$ are harmonic in the lower (upper) half-plane and satisfy the far-field boundary conditions. Substitution into the interface boundary conditions (6.1) results in a set of six ordinary differential equations which can be cast into the form

$$\boldsymbol{J}\boldsymbol{Z}_t = \nabla E(\boldsymbol{Z}), \tag{6.2a}$$

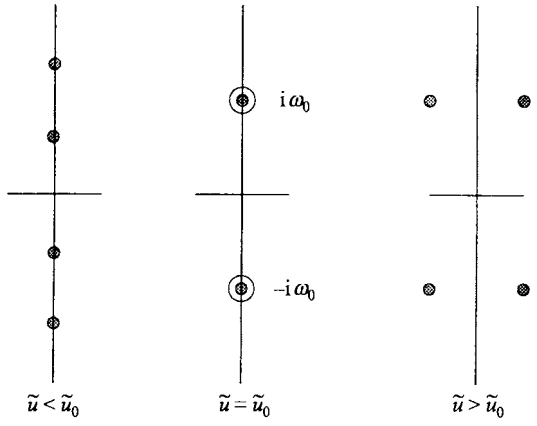

FIGURE 17. Kelvin–Helmholtz instability: a temporal collision of pure imaginary eigenvalues leading to instability.

with

$$Z \overset{\text{def}}{=} \begin{pmatrix} q_1 \\ q_2 \\ e_1 \\ f_1 \\ e_1' \\ f_1' \end{pmatrix} \quad \text{and} \quad \boldsymbol{J} = \begin{bmatrix} 0 & -\rho \boldsymbol{I}_2 & \rho' \boldsymbol{I}_2 \\ \rho \boldsymbol{I}_2 & 0 & 0 \\ -\rho' \boldsymbol{I}_2 & 0 & 0 \end{bmatrix}, \tag{6.2b}$$

where $\boldsymbol{I}_2$ is the identity on $\mathbb{R}^2$. The functional E is the total energy (see Appendix A equations (A 3) and (A 4)) evaluated on the single-mode approximation above:

$$E = \tfrac{1}{2}\rho k(e_1^2+f_1^2)+\tfrac{1}{2}\rho' k(e_1'^2+f_1'^2)-\rho U k(e_1 q_2 - f_1 q_1) + \rho' U' k(e_1' q_2 - f_1' q_1)+\tfrac{1}{2}[(\rho-\rho')g+\sigma k^2](q_1^2+q_2^2). \tag{6.3}$$

Differentiating the energy we find that

$$D^2E(0) = \begin{bmatrix} \theta & 0 & 0 & \rho U k & 0 & -\rho' U' k \\ 0 & \theta & -\rho U k & 0 & \rho' U' k & 0 \\ 0 & -\rho U k & \rho k & 0 & 0 & 0 \\ \rho U k & 0 & 0 & \rho k & 0 & 0 \\ 0 & \rho' U' k & 0 & 0 & \rho' k & 0 \\ -\rho' U' k & 0 & 0 & 0 & 0 & \rho' k \end{bmatrix},$$

where $\theta = (\rho-\rho')g+\sigma k^2$.

The operator $\boldsymbol{J}$ in (6.2) is skew-symmetric but not invertible. The single-mode approximation to the Kelvin–Helmholtz problem has a Hamiltonian formulation but it is a generalized Hamiltonian formulation (Benjamin & Bridges 1992 study the full nonlinear problem and show that it can be transformed in such a way that it has a standard Hamiltonian formulation).

It is interesting to contrast the Hamiltonian structure in (6.2) for the time-dependent problem with the Hamiltonian structure (2.13) for the space-evolution problem. Both problems have a collision-of-eigenvalues singularity although the Kelvin–Helmholtz problem has a collision of temporal eigenvalues while the problem (2.13) has a collision of spatial eigenvalues.

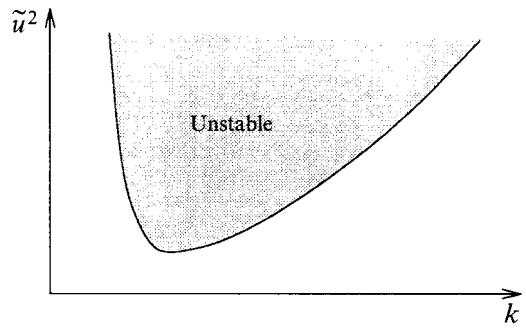

FIGURE 18. The velocity difference $\tilde{u} = U - U'$ between the two fluid layers as a function of wavenumber k showing the Kelvin–Helmholtz unstable region.

Let $\boldsymbol{Z} = \hat{\boldsymbol{X}} e^{\lambda t}$ in (6.2*a*), then the eigenvalue problem for λ is

$$D^2 E(0)\hat{\boldsymbol{Z}} = \lambda \boldsymbol{J}\hat{\boldsymbol{Z}}$$

which is easily solved to find

$$\lambda = \pm i\left\{k\tilde{c}_0 \pm \frac{k}{\rho+\rho'}[\rho\rho'(\tilde{u}_0^2 - \tilde{u}^2)]^{1/2}\right\}, \tag{6.4}$$

where

$$\tilde{u} = U - U', \quad \tilde{c}_0 = \frac{\rho U + \rho' U'}{\rho+\rho'}, \quad \tilde{u}_0^2 = \frac{\rho+\rho'}{\rho\rho'}\left(\sigma k + (\rho-\rho')\frac{g}{k}\right).$$

The eigenvalues in (6.4) are plotted in the complex λ-plane in figure 17 and figure 18 shows the critical curve $\tilde{u}^2 = \tilde{u}_0^2$ in the $(k, \tilde{u}^2)$ plane. In the present case, since the eigenvalue λ is a temporal eigenvalue, when $\mathrm{Re}\,(\lambda) \neq 0$ there is in fact instability (unlike the spatial case in figure 2). The nonlinear bifurcations of periodic travelling waves in the neighbourhood of the Kelvin–Helmholtz instability have been studied recently by Benjamin & Bridges (1992). The similarity of the spatial bifurcation structure for the nonlinear problem in §§3–5 with the temporal bifurcations in the Kelvin–Helmholtz instability is remarkable.

7. Discussion

General properties of steady waves at the interface between two fluids have been presented. A new formulation of the governing equations as a Hamiltonian system leads to new variational principles as well as general results on secondary spatial bifurcations analogous to the superharmonic instability.

Nonlinear interfacial travelling waves in the neighbourhood of the singularity, $c = c_g$, in the linear dispersion relation, have been studied using analytical and numerical methods. New branches of periodic travelling waves were found by analysing a neighbourhood of a second singularity in the nonlinear problem. Basic to the Hamiltonian structure are the integrals $(\bar{F}, \bar{S})$ which are related to the energy flux and the flow force. We showed that the $(\tilde{F}, \bar{S})$-space, where $\tilde{F}$ is the averaged value in space of $\bar{F}$, considered as a two-dimensional parameter space, is a natural diagram on which to plot branches of travelling waves: when the difference in density between both fluids is small, the $(\tilde{F}, \bar{S})$-diagrams contain cusp points which correspond to secondary bifurcations.

In experiments on two-layer flows, there exist parameter values at which such waves could be realized. For example, if one takes the first set of fluids used by Pouliquen *et al.* (1994) in their experiments (water and an equal mixture of silicone oil V2 and 1-2-3-4-tetrahydronaphtalene) which corresponds to $r = 0.0417$, one finds that the wavelength and wave speed corresponding to the minimum of the dispersion curve are $2\pi/k_0 = 6.4$ cm and $c_0 = 9.1$ cm s^{-1}. These values appear to be reasonable values for experiments.

In the invariant spaces, that is parameter values for level sets of the functionals $(\tilde{F}, \tilde{S})$, the transition from the water-wave case ($r = 1$) to the Boussinesq limit ($r \to 0$) has been clearly demonstrated. When the two fluids have comparable densities, both branches of travelling waves which bifurcate from the trivial solution are connected in the form of a swallowtail in the $(\tilde{F}, \tilde{S})$-plane (cf. figures 1 and 2). The presence of a swallowtail in invariant space, as shown in figure 2, is a generally occurring property in the neighbourhood of a collision of a pair of eigenvalues of opposite signature in a Hamiltonian system (see van der Meer 1985, pp. 78–9) or in a reversible system in the presence of a 1:1 resonance (see Iooss & Pérouème 1993). In a nonlinear finite-dimensional Hamiltonian system or in a reversible system with a collision of eigenvalues – in normal form – it is known that the points outside the swallowtail correspond to unbounded solutions while each point in the interior of the swallowtail corresponds to a quasi-periodic state and along the top boundary, between the two cusp points, the stable and unstable manifolds of the hyperbolic periodic orbits are joined to form a heteroclinic. Adapting those results to the present context we can speculate that there exist spatially quasi-periodic travelling waves for this problem and interesting solitary waves with periodic tails not decaying at infinity (see Dias & Iooss 1994). The quasi-periodic travelling waves are natural extensions of the linear quasi-periodic travelling waves. In other words, referring to the dispersion curve in figure 1(*a*), for fixed $c > c_0$ there exist two periodic states of wavenumbers k_1 and k_2 whose combination forms a quasi-periodic state when k_1/k_2 is irrational with waveform $\eta(x) = A_1 e^{ik_1 x} + A_2 e^{ik_2 x}$.

The rigorous existence or linear stability of the periodic waves in §§3–5 has not been considered. However, the linear stability problem is tractable and therefore there are a number of methods that could be used to study the linear stability. For example it should be possible to treat rigorously the existence question and the linear stability question together using Hamiltonian centre manifold theory as in Bridges & Mielke (1995).

The singularity $r = r_0$, which corresponds to the transition between the water-wave case and the Boussinesq limit, has also been studied in detail in this paper. The value r_0 corresponds to a density ratio ρ'/ρ equal to about 0.28. One can imagine that such a density ratio could be obtained experimentally. In addition to the families of periodic waves found here in the neighbourhood of the singularity $c = c_g$ and $r = r_0$, there should also be new branches of solitary waves. Preliminary results indicate that in the transition region there are two kinds of spatially quasi-periodic travelling waves and solitary waves decaying algebraically towards either a periodic state or a uniform flow.

The theory presented in the paper is applicable to more general problems than the ones considered here. The starting point of the paper is the singularity $c = c_g$ and this singularity appears in other contexts. For example in the dynamics of interfacial waves with a current U (cf. Gargett & Hughes 1972; Peregrine 1976, p. 52) the singularity $c_g + U = c$ gives rise to stopping velocities. Associated with the stopping velocities are interesting wave patterns that have also been observed in the open ocean (cf. Gargett & Hughes 1972, figures 1 and 2). The nonlinear structure of such problems should be

similar to that reported here. It has also been shown recently that several phenomena occurring in the propagation of capillary–gravity interfacial waves also occur in the context of internal waves (see for example the paper by Akylas & Grimshaw 1992 on generalized solitary waves) or in the context of large-amplitude gravity waves (Baesens & MacKay 1992). From a theoretical point of view, capillary–gravity interfacial waves have the advantage that secondary bifurcations occur at low amplitude and can therefore be studied analytically.

The work of the first author was carried out while supported by a Research Fellowship from the Alexander von Humboldt Foundation held at the Universität Stuttgart.

Appendix A. Conservation laws and spatial invariants

In this Appendix the four basic conservation laws for the time-dependent two-layer fluid problem are recorded. The channel is confined between two walls at $y = -h'$ and $y = h$. The governing equations are given by (2.1) and the boundary conditions at the walls by (2.2). The pressure in each layer can be obtained from Bernoulli's equation:

$$\rho\phi_t + \tfrac{1}{2}\rho(\phi_x^2 + \phi_y^2) + \rho g y + p = 0$$

in the upper layer and

$$\rho'\phi'_t + \tfrac{1}{2}\rho'(\phi_x'^2 + \phi_y'^2) + \rho' g y + p' = 0$$

in the lower layer. The boundary conditions at the interface $y = \eta(x, t)$ are

$$\eta_t + \phi_x \eta_x - \phi_y = 0, \quad \eta_t + \phi'_x \eta_x - \phi'_y = 0$$

and

$$\rho\phi_t - \rho'\phi'_t + \tfrac{1}{2}\rho(\phi_x^2 + \phi_y^2) - \tfrac{1}{2}\rho'(\phi_x'^2 + \phi_y'^2) + (\rho - \rho')\, g\eta - \sigma w_x = 0.$$

The four basic conservation laws for the time-dependent two-layer fluid problem in a stationary frame of reference are

$$\left.\begin{aligned} \partial m/\partial t + \partial Q/\partial x &= 0 \quad \text{(mass conservation – lower fluid)}, \\ \partial m'/\partial t + \partial Q'/\partial x &= 0 \quad \text{(mass conservation – upper fluid)}, \\ \partial I/\partial t + \partial S/\partial x &= 0 \quad \text{(impulse conservation)}, \\ \partial E/\partial t + \partial F/\partial x &= 0 \quad \text{(energy conservation)}. \end{aligned}\right\} \tag{A 1}$$

The fluxes for the conservation laws are

$$Q = \int_{-h}^{\eta} \rho\phi_x \,\mathrm{d}y, \quad Q' = \int_{\eta}^{h'} \rho'\phi'_x \,\mathrm{d}y, \tag{A 2a, b}$$

$$S = \int_{-h}^{\eta} \tfrac{1}{2}\rho(\phi_x^2 - \phi_y^2)\,\mathrm{d}y + \int_{\eta}^{h'} \tfrac{1}{2}\rho'(\phi_x'^2 - \phi_y'^2)\,\mathrm{d}y - \tfrac{1}{2}(\rho - \rho')\, g\eta^2 + \sigma - \frac{\sigma}{(1+\eta_x^2)^{1/2}} - \int_{-h}^{\eta} \rho\phi_t \,\mathrm{d}y - \int_{\eta}^{h'} \rho'\phi'_t \,\mathrm{d}y, \tag{A 2c}$$

$$F = -\frac{\sigma\eta_t\eta_x}{(1+\eta_x^2)^{1/2}} - \int_{-h}^{\eta} \rho\phi_x\phi_t \,\mathrm{d}y - \int_{\eta}^{h'} \rho'\phi'_x\phi'_t \,\mathrm{d}y. \tag{A 2d}$$

The densities for the conservation laws are

$$m = \rho\eta, \quad m' = -\rho'\eta, \quad I = Q + Q', \quad E = K + V_g + V_\sigma, \tag{A 3}$$

where

$$\left.\begin{aligned} K &= \int_{-h}^{\eta} \tfrac{1}{2}\rho(\phi_x^2+\phi_y^2)\,\mathrm{d}y + \int_{\eta}^{h'} \tfrac{1}{2}\rho'(\phi_x'^2+\phi_y'^2)\,\mathrm{d}y, \\ V_g &= \tfrac{1}{2}(\rho-\rho')g\eta^2, \quad V_\sigma = \sigma[(1+\eta_x^2)^{1/2}-1]. \end{aligned}\right\} \tag{A 4}$$

The conservation laws can be verified by carrying out the differentiation in (A 1)–(A 4) and using the governing equations. Of interest in the present work are the conservation laws when restricted to the moving frame. For states that are steady relative to the frame moving with speed c ($x \mapsto x-ct$), the conservation laws (A 1) reduce to spatial invariants, that is

$$\frac{\mathrm{d}}{\mathrm{d}x}(Q-cm) = \frac{\mathrm{d}}{\mathrm{d}x}(Q'-cm') = 0,$$

$$\frac{\mathrm{d}}{\mathrm{d}x}(S-cI) = \frac{\mathrm{d}}{\mathrm{d}x}(F-cE) = 0.$$

The fourth expression in (A 1) which is called the relative energy flux by Hogan (1983), does not produce an independent spatial invariant. In fact, using (A 2)–(A 4) one finds

$$F-cE = c(S-cI). \tag{A 5}$$

Defining

$$\bar{S} \overset{\text{def}}{=} S-cI = \int_{-h}^{\eta} \tfrac{1}{2}\rho(\phi_x^2-\phi_y^2)\,\mathrm{d}y + \int_{\eta}^{h'} \tfrac{1}{2}\rho'(\phi_x'^2-\phi_y'^2)\,\mathrm{d}y$$
$$-\tfrac{1}{2}(\rho-\rho')g\eta^2+\sigma-\sigma/(1+\eta_x^2)^{1/2}, \tag{A 6a}$$

$$\bar{Q} \overset{\text{def}}{=} Q-cm = -\rho c\eta + \int_{-h}^{\eta} \rho\phi_x\,\mathrm{d}y, \tag{A 6b}$$

$$\bar{Q}' \overset{\text{def}}{=} Q'-cm' = \rho' c\eta + \int_{\eta}^{h'} \rho'\phi_x'\,\mathrm{d}y, \tag{A 6c}$$

it follows that $\bar{S}$, $\bar{Q}$ and $\bar{Q}'$ are absolute spatial invariants for uniformly travelling waves. The set of spatial invariants $\{\bar{S}, \bar{Q}, \bar{Q}'\}$ forms an algebra and so any linear combination of spatial invariants is a spatial invariant. Hence $\bar{Q}_{tot} = \bar{Q}+Q'$ is also a spatial invariant. Hogan (1981) found some relationships between integral properties of capillary–gravity interfacial waves. We denote spatial averages by putting a hat on top of the physical quantity. Some relationships in infinite depth are

$$\hat{I} = 2\hat{K}/c, \quad \hat{S} = 4\hat{K}-3\hat{V}_g-\hat{V}_\sigma, \quad \bar{S} = 2\hat{K}-3\hat{V}_g-\hat{V}_\sigma, \quad \hat{F} = c(3\hat{K}-2\hat{V}_g).$$

The average of the impulse can also be written as

$$\hat{I} = \frac{1}{L}\int -(\rho\Phi-\rho'\Phi')\eta_x\,\mathrm{d}x,$$

where L is the wavelength.

Of interest for the spatial Hamiltonian structure is a quantity closely related to the energy flux F restricted to the moving frame, which is defined as $\bar{F} = F/c-cI$ and which is equal to

$$\bar{F} = \int_{-h}^{\eta} \rho\phi_x(\phi_x-c)\,\mathrm{d}y + \int_{\eta}^{h'} \rho'\phi_x'(\phi_x'-c)\,\mathrm{d}y + \frac{\sigma\eta_x^2}{(1+\eta_x^2)^{1/2}}. \tag{A 7}$$

One easily finds that its spatial average is $\tilde{F} = \hat{K}-2\hat{V}_g$.

Appendix B. Spatial Hamiltonian structure

In this Appendix we record further details about the spatial Hamiltonian structure introduced in §2. For definiteness the formulation, introduced at the beginning of §2, for the finite channel is considered with governing equations (2.13). We will use the notation $\mathscr{H}$ for the Hamiltonian.

By definition a Hamiltonian system is a triple $(\mathscr{M}, \omega_\eta, \mathscr{H})$ where $\mathscr{M}$ is the phase space, ω_η is a non-degenerate closed two-form and $\mathscr{H}: \mathscr{M} \to \mathbb{R}$ is the Hamiltonian functional. In the present case the phase space consists of functions of the form (2.12) where the first four components are real numbers with $-h < \eta < h'$, the fourth and fifth components are defined on $y \in (-h, \eta)$ and the last two components are defined on $y \in (\eta, h')$. Associated with such functions are the boundary conditions (2.2) and (2.9). The inner product for elements in the phase space is defined in (2.15).

The skew-symmetric operator $\boldsymbol{K}(\boldsymbol{Z})$ defined the two-form ω_η and a necessary condition for a Hamiltonian structure is that ω_η be closed. The skew-symmetry of $\boldsymbol{K}(\boldsymbol{Z})$ is verified by noting that

$$\langle \boldsymbol{U}, \boldsymbol{K}(\boldsymbol{Z})\, \boldsymbol{V} \rangle_\eta = -\langle \boldsymbol{K}(\boldsymbol{Z})\, \boldsymbol{U}, \boldsymbol{V} \rangle_\eta.$$

The two-form ω_η is defined by the identification

$$\omega_\eta(\boldsymbol{U}, \boldsymbol{V}) = \langle \boldsymbol{K}(\boldsymbol{Z})\, \boldsymbol{U}, \boldsymbol{V} \rangle_\eta$$

resulting in

$$\omega_\eta = \sigma\, \mathrm{d}w \wedge \mathrm{d}\eta - \mathscr{u}\, \mathrm{d}\Phi \wedge \mathrm{d}\eta + \mathscr{u}'\, \mathrm{d}\Phi' \wedge \mathrm{d}\eta + \int_{-h}^{\eta} (\mathrm{d}u \wedge \mathrm{d}\phi)\, \mathrm{d}y + \int_{\eta}^{h'} (\mathrm{d}u' \wedge \mathrm{d}\phi')\, \mathrm{d}y. \tag{B 1}$$

The two-form ω_η is closed if $\mathrm{d}\omega_\eta = 0$ where d represents exterior differentiation. To verify closure we show that ω_η is exact. Let

$$\alpha_\eta = \sigma w\, \mathrm{d}\eta + \int_{-h}^{\eta} (u\, \mathrm{d}\phi)\, \mathrm{d}y + \int_{\eta}^{h'} (u'\, \mathrm{d}\phi')\, \mathrm{d}y. \tag{B 2}$$

Then using the properties of the exterior derivative we find

$$\begin{aligned} \mathrm{d}\alpha_\eta &= \sigma\, \mathrm{d}w \wedge \mathrm{d}\eta + \mathrm{d}\eta \wedge (u\, \mathrm{d}\phi)|_{y=\eta} - \mathrm{d}\eta \wedge (u'\, \mathrm{d}\phi')|_{y=\eta} \\ &\quad + \int_{-h}^{\eta} \mathrm{d}u \wedge \mathrm{d}\phi\, \mathrm{d}y + \int_{\eta}^{h'} \mathrm{d}u' \wedge \mathrm{d}\phi'\, \mathrm{d}y \\ &= \omega_\eta \end{aligned}$$

and since $\mathrm{d}\,\mathrm{d}\alpha_\eta = 0$ it follows that ω_η is closed.

The one-form α_η in (B 2) is the basic one-form or (spatial) action for the Hamiltonian structure and it is related to the energy flux. Parametrizing α_η by x results in

$$\alpha_\eta^* = \sigma w \eta_x + \int_{-h}^{\eta} (u\phi_x)\, \mathrm{d}y + \int_{\eta}^{h'} (u'\phi_x')\, \mathrm{d}y$$

which is related to the energy flux relative to a moving frame (cf. (A 7)).

The governing equation for the Hamiltonian system is given abstractly by

$$\boldsymbol{Z}_x = \boldsymbol{X}(\boldsymbol{Z}), \tag{B 3}$$

where $\boldsymbol{X}(\boldsymbol{Z})$ is defined by

$$\omega_\eta(\boldsymbol{X}, \xi) = \langle \nabla \mathscr{H}(\boldsymbol{Z}), \xi \rangle_\eta \tag{B 4}$$

for all admissible ξ. However, since $\boldsymbol{K}(\boldsymbol{Z})$ is not invertible we write (B 3) in the form

$$\boldsymbol{K}(\boldsymbol{Z})\, \boldsymbol{Z}_x = \nabla \mathscr{H}(\boldsymbol{Z}). \tag{B 5}$$

The kernel of $\boldsymbol{K}(\boldsymbol{Z})$, defined in (2.12), is two-dimensional with

$$\mathrm{Ker}\{\boldsymbol{K}(\boldsymbol{Z})\} = \mathrm{span}\{\zeta, \zeta'\} \quad \text{where} \quad \begin{cases} \zeta = (\sigma, 0, 0, u, 0, 0, 0, 0)^T \\ \zeta' = (0, \sigma, 0, -u', 0, 0, 0, 0)^T. \end{cases} \tag{B 6}$$

Therefore (B 5) is subject to the conditions

$$0 = \langle \zeta, \boldsymbol{K}(\boldsymbol{Z})\, \boldsymbol{Z}_x \rangle_\eta = \langle \zeta, \nabla \mathscr{H}(\boldsymbol{Z}) \rangle_\eta$$
$$0 = \langle \zeta', \boldsymbol{K}(\boldsymbol{Z})\, \boldsymbol{Z}_x \rangle_\eta = \langle \zeta', \nabla \mathscr{H}(\boldsymbol{Z}) \rangle_\eta$$

and

$$\left.\begin{aligned} \langle \zeta, \nabla \mathscr{H}(\boldsymbol{Z}) \rangle_\eta = \langle \zeta, \nabla \bar{S}(\boldsymbol{Z}) \rangle_\eta = \sigma \left(-\rho \phi_y|_{y=\eta} + \frac{wu}{(1-w^2)^{1/2}} \right) = 0 \\ \langle \zeta', \nabla \mathscr{H}(\boldsymbol{Z}) \rangle_\eta = \langle \zeta', \nabla \bar{S}(\boldsymbol{Z}) \rangle_\eta = \sigma \left(\rho' \phi'_y|_{y=\eta} - \frac{wu'}{(1-w^2)^{1/2}} \right) = 0. \end{aligned}\right\} \tag{B 7}$$

Therefore these last two equations are constraints. They are reformulations, in terms of the new coordinates, of the kinematic conditions. Note however that when $\sigma = 0$ the constraints are automatically satisfied.

Finally, in this Appendix, the relations between symmetries and conservation laws for the spatial Hamiltonian system are considered. Let

$$V = \begin{pmatrix} 1 \\ 0 \\ 0 \\ 0 \\ 1 \\ 0 \\ 0 \\ 0 \end{pmatrix} \quad \text{and} \quad V' = \begin{pmatrix} 0 \\ 1 \\ 0 \\ 0 \\ 0 \\ 0 \\ 1 \\ 0 \end{pmatrix}. \tag{B 8}$$

Then $\boldsymbol{Z} + \epsilon \boldsymbol{V}$ is the group action corresponding to constant perturbation of the potential ϕ and $\boldsymbol{Z} + \epsilon' \boldsymbol{V}'$ is the group action corresponding to constant perturbation of the potential ϕ'. It is precisely these two symmetries that generate the conserved quantities $\bar{Q}$ and $\bar{Q}'$. The connection is established using Noether's theorem adapted to the spatial setting (cf. Bridges 1994, Appendix A). First note the identities

$$\boldsymbol{K}(\boldsymbol{Z})\, \boldsymbol{V} = \nabla \bar{Q}(\boldsymbol{Z}) \quad \text{and} \quad \boldsymbol{K}(\boldsymbol{Z})\, \boldsymbol{V}' = \nabla \bar{Q}'(\boldsymbol{Z}) \tag{B 9}$$

which follow from the definition of $\boldsymbol{K}(\boldsymbol{Z})$ (in (2.12)) and from

$$\nabla \bar{Q}(\boldsymbol{Z}) = \begin{pmatrix} 0 \\ 0 \\ u \\ 0 \\ 0 \\ 0 \\ 1 \\ 0 \\ 0 \end{pmatrix} \quad \text{and} \quad \nabla \bar{Q}'(Z) = \begin{pmatrix} 0 \\ 0 \\ -u' \\ 0 \\ 0 \\ 0 \\ 0 \\ 0 \\ 1 \end{pmatrix}. \tag{B 10}$$

Now, since $\mathscr{H}(Z)$ is invariant under constant perturbation of the potential ϕ: $\mathscr{H}(Z+\epsilon V) = \mathscr{H}(Z)$ for all $\epsilon \in \mathbb{R}$, it follows that

$$\begin{aligned} 0 = \frac{\mathrm{d}}{\mathrm{d}\epsilon}\mathscr{H}(Z+\epsilon V)\Big|_{\epsilon=0} &= \langle \nabla\mathscr{H}(Z), V\rangle_\eta \\ &= \langle \boldsymbol{K}(Z)\, Z_x, V\rangle_\eta \\ &= -\langle Z_x, \boldsymbol{K}(Z)\, V\rangle_\eta \\ &= -\langle Z_x, \nabla\bar{Q}(Z)\rangle_\eta \\ &= -\mathrm{d}\bar{Q}/\mathrm{d}x \end{aligned}$$

using (B 5), skew-symmetry of $\boldsymbol{K}(Z)$ and the first identity in (B 9). This verifies that $\bar{Q}$ is indeed a spatial invariant. In other words the spatial formulation of Noether's relation (B 9) implies the spatial invariance of $\bar{Q}$. A similar argument verifies that $\bar{Q}'_x = 0$.

Appendix C. Uniform flows and criticality

In this Appendix, we consider steady flows in a stationary frame of reference with a current β in the lower layer and β' in the upper layer. The governing equations are the same as in §2, except for the boundary conditions at the interface

$$\left.\begin{aligned} (\beta+\phi_x)\,\eta_x - \phi_y = 0 \\ (\beta'+\phi'_x)\,\eta_x - \phi'_y = 0 \end{aligned}\right\} \quad \text{at} \quad y = \eta(x) \tag{C 1}$$

and

$$\tfrac{1}{2}\rho[(\beta+\phi_x)^2+\phi_y^2] - \tfrac{1}{2}\rho'[(\beta'+\phi'_x)^2+\phi'^2_y] + (\rho-\rho')\,g\eta - \sigma w_x = R. \tag{C 2}$$

Following the same steps as in §2 with essentially replacing c by $-\beta$ (resp. $-\beta'$) in the lower fluid (resp. upper fluid), one obtains a spatial Hamiltonian formulation similar to (2.13), which can be written in the form

$$\boldsymbol{K}(Z)\, Z_x = \nabla\mathscr{H}(Z) = \nabla S(Z) - \beta\nabla Q(Z) - \beta'\nabla Q'(Z), \tag{C 3}$$

where

$$Q = \int_{-h}^{\eta} u\,\mathrm{d}y, \quad Q' = \int_{\eta}^{h'} u'\,\mathrm{d}y, \tag{C 4a}$$

$$\begin{aligned} S = &\int_{-h}^{\eta} \frac{1}{2}\left(\frac{1}{\rho}u^2 - \rho\phi_y^2\right)\mathrm{d}y + \int_{\eta}^{h'} \frac{1}{2}\left(\frac{1}{\rho'}u'^2 - \phi'^2_y\right)\mathrm{d}y \\ &+ R\eta - \tfrac{1}{2}(\rho-\rho')\,g\eta^2 + \sigma[1-(1-w^2)^{1/2}]. \end{aligned} \tag{C 4b}$$

The Hamiltonian formulation (C 3) leads to an interesting variational principle for uniform flows. Uniform flows are steady states that are also x-independent. It is evident from (C 3) that such states satisfy

$$\nabla S(Z) - \beta\nabla Q(Z) - \beta'\nabla Q'(Z) = 0 \tag{C 5}$$

for some constants β and β'. Equation (C 5) can be characterized as the Lagrange necessary condition for the following constrained variational principle. Let q and q' be level sets of the mass flux functionals Q and Q'. Then uniform flows, with R fixed, of the two-layer fluid problem in a finite channel correspond to critical points of the flow force restricted to level sets of the mass fluxes:

$$\mathrm{crit}\,(S)|_{Q=q,\, Q'=q'}, \tag{C 6}$$

with Lagrange necessary condition (C 5). Solving the Lagrange necessary condition using the gradients of the functionals (C 4) results in

$$u = \rho\beta, \quad u' = \rho'\beta', \quad \eta = \bar{\eta}. \tag{C 7a}$$

where

$$\bar{\eta} = \frac{1}{(\rho-\rho')g}(R - \tfrac{1}{2}\rho\beta^2 + \tfrac{1}{2}\rho'\beta'^2) \tag{C 7b}$$

and R is considered arbitrary but specified.

Note that an elementary consequence of the Lagrange multiplier theory is

$$\beta = \frac{\partial S}{\partial q} \quad \text{and} \quad \beta' = \frac{\partial S}{\partial q'}; \tag{C 8}$$

that is, the flow velocities β and β' are given by slopes in the flow force and mass flux parameter space. It follows from (C 8) that

$$\begin{pmatrix} \partial\beta/\partial q & \partial\beta/\partial q' \\ \partial\beta'/\partial q & \partial\beta'/\partial q' \end{pmatrix} = \begin{pmatrix} \partial^2 S/\partial q^2 & \partial^2 S/\partial q\,\partial q' \\ \partial^2 S/\partial q'\,\partial q & \partial^2 S/\partial q'^2 \end{pmatrix}. \tag{C 9}$$

An interesting consequence of the above variational principle is that critical flows can be defined by the condition

$$\det\begin{bmatrix} \partial Q/\partial\beta & \partial Q/\partial\beta' \\ \partial Q'/\partial\beta & \partial Q'/\partial\beta' \end{bmatrix} = 0. \tag{C 10}$$

This is verified as follows. Using (C 4) and (C 7) the mass fluxes evaluated at the uniform flow are

$$Q = \rho H\beta \quad \text{and} \quad Q' = \rho' H'\beta',$$

where $H = \bar{\eta} + h$ and $H' = h' - \bar{\eta}$. Noting that $\bar{\eta}$ depends on β and β' via (C 7) the Jacobian is

$$\begin{pmatrix} \dfrac{\partial Q}{\partial\beta} & \dfrac{\partial Q}{\partial\beta'} \\ \dfrac{\partial Q'}{\partial\beta} & \dfrac{\partial Q'}{\partial\beta'} \end{pmatrix} = \begin{pmatrix} \rho H\left(1 - \dfrac{\rho\beta^2}{(\rho-\rho')gH}\right) & \dfrac{\rho\rho'\beta\beta'}{(\rho-\rho')g} \\ \dfrac{\rho\rho'\beta\beta'}{(\rho-\rho')g} & \rho' H'\left(1 - \dfrac{\rho'\beta'^2}{(\rho-\rho')gH}\right) \end{pmatrix}$$

and therefore

$$\det\begin{bmatrix} \dfrac{\partial Q}{\partial B} & \dfrac{\partial Q}{\partial\beta'} \\ \dfrac{\partial Q'}{\partial\beta} & \dfrac{\partial Q'}{\partial\beta'} \end{bmatrix} = \rho\rho' HH'\left[1 - \frac{\rho}{\rho-\rho'}\frac{\beta^2}{gH} - \frac{\rho'}{\rho-\rho'}\frac{\beta'^2}{gH'}\right]. \tag{C 11}$$

Define Froude numbers for the lower and upper layers by

$$F^2 = \frac{\beta^2}{gH} \quad \text{and} \quad F'^2 = \frac{\beta'^2}{gH'}.$$

Then the condition (C 10) applied to (C 11) leads to

$$\frac{\rho}{\rho-\rho'}F^2 + \frac{\rho'}{\rho-\rho'}F'^2 = 1,$$

which is the well-known condition for criticality (cf. Mehrota & Kelly 1973, equation (4)). It also follows from (C 9) that critical flows give rise to a singularity in the Hessian of the flow force with respect to the mass fluxes. Indeed, the variational principle (C 6) is singular precisely at criticality.

Appendix D. A variational principle for periodic waves coupled with a mean flow

When mean flow effects are important, as in the case of a periodic travelling wave in a finite-width channel, the variational principle of §3 for periodic travelling waves can be generalized. Here we present a variational principle for periodic travelling waves in a finite channel. The coordinate system for the channel cross-section, introduced at the beginning of §2, is used where $y = -h (y = h')$ at the lower (upper) wall and $y = \eta$ separates the two fluids. In order to incorporate mean elevation changes the Bernoulli constant R in (2.4) is no longer assumed to be known and mean flows β and β' are incorporated in the equations (see Appendix C). The $R\eta$ term is separated from the flow force definition in (C 4). Therefore, in this Appendix, the flow force and excess mass density are

$$\left.\begin{aligned} S(\boldsymbol{Z}) &= \int_{-h}^{\eta} \frac{1}{2}\left(\frac{1}{\rho}u^2 - \rho\phi_y^2\right)\mathrm{d}y + \int_{\eta}^{h'} \frac{1}{2}\left(\frac{1}{\rho'}u'^2 - \tfrac{1}{2}\rho'\phi_y'^2\right)\mathrm{d}y \\ &\quad -\tfrac{1}{2}(\rho-\rho')g\eta^2 + \sigma[1-(\sqrt{1-w^2})^{1/2}], \\ P(\boldsymbol{Z}) &= \eta. \end{aligned}\right\} \tag{D 1}$$

The governing equation (C 3) then takes the form

$$\boldsymbol{K}(\boldsymbol{Z})\,\boldsymbol{Z}_x = \nabla S(\boldsymbol{Z}) + R\nabla P(\boldsymbol{Z}) - \beta\nabla Q(\boldsymbol{Z}) - \beta'\nabla Q'(\boldsymbol{Z}), \tag{D 2}$$

with $Q(\boldsymbol{Z})$ and $Q'(\boldsymbol{Z})$ as defined in (C 4). However by scaling $x \mapsto kx$ so that k appears in the equation, as in §3, the governing equation becomes

$$k\boldsymbol{K}(\boldsymbol{Z})\,\boldsymbol{Z}_x = \nabla S(\boldsymbol{Z}) + R\nabla P(\boldsymbol{Z}) - \beta\nabla Q(\boldsymbol{Z}) - \beta'\nabla Q'(\boldsymbol{Z}). \tag{D 3}$$

But $\boldsymbol{K}(\boldsymbol{Z})\,\boldsymbol{Z}_x$ is the gradient of the spatial action with density

$$B(\boldsymbol{Z}) = \int_{-h}^{\eta} u\phi_x\,\mathrm{d}y + \int_{\eta}^{h'} u'\phi_x'\,\mathrm{d}y + \sigma w\eta_x. \tag{D 4}$$

With respect to the inner product (2.15), including also integration over x, $\nabla B(\boldsymbol{Z}) = \boldsymbol{K}(\boldsymbol{Z})\,\boldsymbol{Z}_x$ and therefore (D 3) is equivalent to

$$\nabla Y(Z; k, R, \beta, \beta') = 0 \tag{D 5a}$$

with

$$Y(\boldsymbol{Z}; k, R, \beta, \beta') = \int_0^{2\pi} [S(\boldsymbol{Z}) - kB(\boldsymbol{Z}) + RP(\boldsymbol{Z}) - \beta Q(\boldsymbol{Z}) - \beta' Q'(\boldsymbol{Z})]\,\mathrm{d}x. \tag{D 5b}$$

Equation (D 5) is the Lagrange necessary condition for the following constrained variational principle: *periodic travelling waves with coupled mean-flow effects correspond to critical points of the flow force restricted to level sets of the spatial action, mean elevation and mass fluxes*:

$$\mathrm{crit}\,(S)|_{\hat{B}=b,\,\hat{P}=p,\,\hat{Q}=q,\,\hat{Q}'=q'} \tag{D 6}$$

where the hat indicates averaging over x from 0 to 2π.

The Lagrange multiplier theory leads immediately to the interesting identities

$$k = \frac{\partial S}{\partial b}, \quad R = -\frac{\partial S}{\partial p}, \quad \beta = \frac{\partial S}{\partial q}, \quad \beta' = \frac{\partial S}{\partial q'}, \tag{D 7}$$

and

$$\begin{pmatrix} \frac{\partial k}{\partial b} & \frac{\partial k}{\partial p} & \frac{\partial k}{\partial q} & \frac{\partial k}{\partial q'} \\ -\frac{\partial R}{\partial b} & -\frac{\partial R}{\partial p} & -\frac{\partial R}{\partial q} & -\frac{\partial R}{\partial q'} \\ \frac{\partial \beta}{\partial b} & \frac{\partial \beta}{\partial p} & \frac{\partial \beta}{\partial q} & \frac{\partial \beta}{\partial q'} \\ \frac{\partial \beta'}{\partial b} & \frac{\partial \beta'}{\partial p} & \frac{\partial \beta'}{\partial q} & \frac{\partial \beta'}{\partial q'} \end{pmatrix} = \mathrm{Hess}_I(S); \quad I = (b, p, q, q'),$$

where $\mathrm{Hess}_I(S)$ is the 4×4 Hessian of S with respect to I. The minus sign is due to convention (the way the Bernoulli constant is defined).

The constrained variational principle (D 6) is non-degenerate at a given state if $\det[\mathrm{Hess}_I(S)] \neq 0$. The above variational principle is a generalization of the variational principle for uniform flows, (C 6), to the case of periodic waves coupled to the mean flow. The above variational principle can be used to organize the parameter structure in numerical computations, such as those in §5 when the fluid is of finite depth, when coupled mean flow effects are important.

REFERENCES

AKYLAS, T. R. 1993 Envelope solitons with stationary crests. *Phys. Fluids* A **5**, 789–791.

AKYLAS, T. R. & GRIMSHAW, R. H. T. 1992 Solitary internal waves with oscillatory tails. *J. Fluid Mech.* **242**, 279–298.

BAESENS, C. & MACKAY, R. S. 1992 Uniformly travelling water waves from a dynamical systems viewpoint: some insights into bifurcations from Stokes' family, *J. Fluid Mech.* **241**, 333–347.

BENJAMIN, T. B. 1984 Impulse, flow force and variational principles. *IMA J. Appl. Maths* **32**, 3–68.

BENJAMIN, T. B. 1992 A new kind of solitary wave. *J. Fluid Mech.* **245**, 401–11.

BENJAMIN, T. B. & BRIDGES, T. J. 1992 Reappraisal of the Kelvin–Helmholtz problem. Part I: Hamiltonian structure, Part II: Travelling waves and bifurcations. Preprint, University of Oxford (*J. Fluid Mech.* submitted).

BENJAMIN, T. B. & OLVER, P. J. 1982 Hamiltonian structure, symmetries and conservation laws for water waves. *J. Fluid Mech.* **125**, 137–185.

BONTOZOGLOU, V. & HANRATTY, T. J. 1990 Capillary–gravity Kelvin–Helmholtz waves close to resonance. *J. Fluid Mech.* **217**, 71–91.

BRIDGES, T. J. 1990 Bifurcation of periodic solutions near a collision of eigenvalues of opposite signature. *Math. Proc. Camb. Phil. Soc.* **108**, 575–601.

BRIDGES, T. J. 1991 Stability of periodic solutions near a collision of eigenvalues of opposite signature. *Math. Proc. Camb. Phil. Soc.* **109**, 375–403.

BRIDGES, T. J. 1992*a* Hamiltonian bifurcations of the spatial structure for coupled nonlinear Schrödinger equations. *Physica* D **57**, 375–394.

BRIDGES, T. J. 1992*b* Spatial Hamiltonian structure, energy flux and the water-wave problem. *Proc. R. Soc. Lond.* A **439**, 297–315.

BRIDGES, T. J. 1994 Hamiltonian spatial structure for 3D water-waves relative to a moving frame of reference. *J. Nonlinear Sci.* **4**, 221–251.

BRIDGES, T. J. & MIELKE, A. 1995 A proof of the Benjamin–Feir instability. *Arch. Rat. Mech. Anal.* (to appear).

BRYDEN, H. L. & KINDER, T. H. 1991 Steady two-layer exchange through the Straight of Gibraltar. *Deep-Sea Res.* **38** (Supplement 1), S445–S463.

DEPRIT, A. & HENRARD, J. 1968 A manifold of periodic orbits. *Adv. Astron. Astrophys.* **6**, 1–124.

DIAS, F. & BRIDGES, T. J. 1994 Geometric aspects of spatially periodic interfacial waves. *Stud. Appl. Maths* **93**, 93–132.

DIAS, F. & IOOSS, G. 1993 Gravity–capillary solitary waves with damped oscillations. *Physica* D **65**, 399–423.

DIAS, F. & IOOSS, G. 1994 Ondes solitaires 'noires' à l'interface entre deux fluides en présence de tension superficielle. *C. R. Acad. Sci. Paris I* **319**, 89–93.

GARGETT, A. E. & HUGHES, B. A. 1972 On the interactions of surface and internal waves. *J. Fluid Mech.* **52**, 179–191.

GOLUBITSKY, M. & SCHAEFFER, D. 1985 *Singularities and Groups in Bifurcation Theory*, Vol. I. Springer.

HOGAN, S. J. 1981 Relationships between integral properties of gravity–capillary interfacial waves. *Phys. Fluids* **24**, 774–775.

HOGAN, S. J. 1983 Energy flux in capillary-gravity waves. *Phys. Fluids* **26**, 1206–1209.

IOOSS, G. & KIRCHGÄSSNER, K. 1990 Bifurcation d'ondes solitaires en présence d'une faible tension superficielle'. *C. R. Acad. Sci. Paris I* **311**, 265–268.

IOOSS, G. & PÉROUÈME, M.-C. 1993 Perturbed homoclinic solutions in reversible 1:1 resonance vector fields. *J. Diffl Equat.* **102**, 62–88.

KOOP, C. G. & REDEKOPP, L. G. 1981 The interaction of long and short internal gravity waves: theory and experiment. *J. Fluid Mech.* **111**, 367–409.

LONGUET-HIGGINS, M. S. 1985 Bifurcation in gravity waves. *J. Fluid Mech.* **151**, 457–475.

LONGUET-HIGGINS, M. S. 1993 Capillary–gravity waves of solitary type and envelope solitons on deep water. *J. Fluid Mech.* **252**, 703–711.

MEER, J. C. VAN DER 1985 *The Hamiltonian Hopf Bifurcation*, Lecture Notes in Mathematics vol. 1160. Springer.

MEHROTA, S. C. & KELLY, R. E. 1973 On the question of non-uniqueness of internal hydraulic jumps and drops in a two-fluid system. *Tellus* **25**, 560–567.

MIELKE, A. 1991 *Hamiltonian and Lagrangian Flows On Center Manifolds*, Lecture Notes in Mathematics, vol. 1489. Springer.

PEREGRINE, D. H. 1976 Interactions of water waves and currents. *Adv. Appl. Mech.* **16**, 9–117.

PEREGRINE, D. H. & THOMAS, G. P. 1979 Finite-amplitude deep-water waves on currents. *Phil. Trans. R. Soc. Lond.* A **292**, 371–390.

POULIQUEN, O., CHOMAZ, J. M. & HUERRE, P. 1994 Propagating Holmboe waves at the interface between two immiscible fluids. *J. Fluid Mech.* **266**, 277–302.

PULLIN, D. I. & GRIMSHAW, R. H. 1983 Nonlinear interfacial progressive waves near a boundary in a Boussinesq fluid. *Phys. Fluids* **26**, 897–905.

SAFFMAN, P. G. 1985 The superharmonic instability of finite-amplitude water waves. *J. Fluid Mech.* **159**, 169–174.

SAFFMAN, P. G. & YUEN, H. C. 1982 Finite-amplitude interfacial waves in the presence of a current. *J. Fluid Mech.* **123**, 459–476.

THORPE, S. A. 1969 Experiments on the instability of stratified shear flows: immiscible fluids. *J. Fluid Mech.* **39**, 25–48.

VANDEN-BROECK, J.-M. & DIAS, F. 1992 Gravity–capillary solitary waves in water of infinite depth and related free surfaced flows. *J. Fluid Mech.* **240**, 549–557.

WHITHAM, G. B. 1974 *Linear and Nonlinear Waves*. Wiley-Interscience.

ZAKHAROV, V. E. 1968 Stability of periodic waves of finite amplitude on the surface of a deep fluid. *Zh. Prikl. Mekh. Fiz.* **9**, 86–94 (English transl: *J. Appl. Mech. Tech. Phys.* **2**, 190–194).

ZUFIRIA, J. A. 1987 Symmetry breaking in periodic and solitary gravity–capillary waves on water of finite depth. *J. Fluid Mech.* **184**, 183–206.